Wu Q., Suzuki J.S., Zaha H., Lin T-M., Peterson RE.,	Tohyama C., Ohsako S. Differences in gene expression and benzo[a]pyrene-induced DNA adduct formation in the liver of three strains of female mice with identical *AhRb2* genotype treated with 2,3,7,8-tetrachlorodibenzo-*p*-dioxin and/or benzo[a]pyrene.	*J Applied Toxicol*	8	724-733,	2008
Yukuto Yasuhiko, Satoshi Kitajima, Yu Takahashi, Masayuki Oginuma, Harumi Kagiwada, Jun Kanno, and Yumiko	Functional importance of evolutionally conserved Tbx6 binding sites in the presomitic mesoderm-specific enhancer of Mesp2.	Development	Vol.135, No.21	3511-3519	2008
Kamata, R., Shiraishi, F., Nishikawa, J., Yonemoto, J. ,Shiraishi, H.	Screening and detection of the in vitro agonistic activity of xenobiotics on the retinoic acid receptor.	Toxicol In Vitro	22	1050-1061	2008
Nishimura, N., Matsumura, F., Vogel, C. F., Nishimura, H., Yonemoto,	C. (2008) Critical role of cyclooxygenase-2 activation in pathogenesis of hydronephrosis caused by lactational exposure of mice to dioxin.	Toxicol Appl Pharma	231	374-383	2008
Sone, H. Yonemoto, J	A genome imformatics and epidemiological study identifies alleles in ARNT2 associated with risk of hypospadias and micropenis. Organohalogen	Compounds	70	1004-1007	2008
Yonemoto, J., Kawahara, J., Hattori, T., Matsumura, T. Sugama, S.	Concentration of PCBs and OH-PCBs in preserved umbilical cords.	Organohalogen Compounds	70,	2436-2438	2008

書籍

著者氏名	論文タイトル名	書籍全体の編集者名	書籍名	出版社名	出版地	出版年	ページ
洲鎌盛一	熱性けいれんで来院した児に必要な検査は何か？	真部　淳、上村克徳　編集	小児科研修の素朴な疑問に答えます	メディカル・サイエンス・インターナショナル	東京	2008年5月	
洲鎌盛一	単純型熱性けいれんにジアゼパム座薬の投与は必要か？	真部　淳、上村克徳　編集	小児科研修の素朴な疑問に答えます	メディカル・サイエンス・インターナショナル	東京	2008年5月	
洲鎌盛一	子どもの睡眠。入眠時の気になる行動		小児内科	東京医学者	東京	2008年5月	
洲鎌盛一	成長と発達	斉藤理恵子、早坂素子、西海真理。編集	小児看護ポケットナビ	中山書店	東京	2008年7月	
洲鎌盛一	胃食道逆流症を伴い長期に経管栄養を必要とした22q11.2欠失症候群の症例	里宇明元、藤原俊之。編集　植松宏、太田哲生、大塚友	ケーススタデイ摂食・嚥下リハビリテーション50症例から学ぶ実践的アプロー	医歯薬出版	東京	2008年9月	
洲鎌盛一	体重増加不良(FTT)と発達障害	松井陽	成育医療センターメールマガジン	国立成育医療センター	東京	2008年3月3日	
洲鎌盛一	おしゃぶりの使用		ケータイ家庭の医学	保健同人社	東京	2008, 8月	
洲鎌盛一	繰り返す自家中毒の予防法		ケータイ家庭の医学	保健同人社	東京	2008, 11月	
洲鎌盛一	アスペルガー症候群		ケータイ家庭の医学	保健同人社	東京	2008, 12月	

研究成果の刊行物・別刷り

THE JOURNAL OF BIOLOGICAL CHEMISTRY VOL. 283, NO. 9, pp. 5525–5532, February 29, 2008

Mastermind-like Domain-containing 1 (*MAMLD1* or *CXorf6*) Transactivates the *Hes3* Promoter, Augments Testosterone Production, and Contains the SF1 Target Sequence*[S]

Received for publication, April 19, 2007, and in revised form, December 27, 2007 Published, JBC Papers in Press, December 27, 2007, DOI 10.1074/jbc.M703289200

Maki Fukami[‡1], Yuka Wada[‡], Michiyo Okada[‡], Fumiko Kato[‡], Noriyuki Katsumata[‡], Takashi Baba[§], Ken-ichirou Morohashi[§], Jocelyn Laporte[¶], Motoo Kitagawa[‖], and Tsutomu Ogata[‡]

From the [‡]Department of Endocrinology and Metabolism, National Research Institute for Child Health and Development, Tokyo 157-8535, Japan, [§]Division for Sex Differentiation, National Institute for Basic Biology, Okazaki 444-8787, Japan, [¶]Department of Molecular Pathology, Institut de Génétique et de Biologie Moléculaire et Cellulaire, Illkirch 67404, France, and [‖]Department of Molecular and Tumor Pathology, Chiba University Graduate School of Medicine, Chiba 260-8670, Japan

Although chromosome X open reading frame 6 (*CXorf6*) has been shown to be a causative gene for hypospadias, its molecular function remains unknown. To clarify this, we first examined CXorf6 protein structure, identifying homology to mastermind-like 2 (MAML2) protein, which functions as a co-activator in canonical Notch signaling. Transactivation analysis for wild-type CXorf6 protein by luciferase assays showed that CXorf6 significantly transactivated the promoter of a noncanonical Notch target gene hairy/enhancer of split 3 (*Hes3*) without demonstrable DNA-binding capacity. Transactivation analysis was also performed for the previously described three apparently pathologic nonsense mutations, indicating that E124X and Q197X proteins had no transactivation function, whereas R653X protein retained a nearly normal transactivation function. Subcellular localization analysis revealed that wild-type and R653X proteins co-localized with MAML2 protein in nuclear bodies, whereas E124X and Q197X proteins were incapable of localizing to nuclear bodies. Thus, further studies were performed for R653X, revealing the occurrence of nonsense mediated mRNA decay *in vivo*. Next, transient knockdown of *CXorf6* was performed using small interfering RNA, showing reduced testosterone production in mouse Leydig tumor cells. Furthermore, steroidogenic factor 1 (SF1) protein bound to a specific sequence in the upstream of the *CXorf6* coding region and exerted a transactivation activity. These results suggest that *CXorf6* transactivates the *Hes3* promoter, augments testosterone production, and contains the SF1 target sequence, thereby providing the first clue to clarify the biological role of *CXorf6*. We designate *CXorf6* as *MAMLD1* (mastermind-like domain-containing 1) based on its characteristic structure.

Chromosome X open reading frame 6 (*CXorf6*)[2] was identified by Laporte *et al.* (1, 2) as a candidate gene for 46,XY disorders of sex development. It spans ~70 kb in genomic sequence and comprises at least seven exons. An open reading frame resides on exons 3–6 and produces two proteins of 701 and 660 amino acids because of in-frame alternative splicing with and without exon 4. PCR-based human cDNA library screening has revealed ubiquitous expression of both splice variants, with the exon 4 positive variant being the major form (3). To date, however, the products of *CXorf6* have been poorly characterized, although glutamine- and proline-rich domains have been identified on exon 3 (1).

We have recently shown that *CXorf6* is a causative gene for hypospadias (3), a common male external genital anomaly defined by the urethral opening on the ventral side of the penis and classified into several types on the basis of the anatomical location of the urethral meatus (4). This notion is based primarily on the identification of nonsense mutations in two maternally related half-brothers (E124X) and in two sporadic boys (Q197X and R653X) with penoscrotal hypospadias (3). Because the mouse homolog (G630014P10Rik, NM_001081354) is transiently expressed in fetal Sertoli and Leydig cells around the critical period for sex development, it is likely that the *CXorf6* mutations cause hypospadias primarily because of testicular dysfunction and the resultant compromised testosterone production around that period (3). Indeed, although various genetic and environmental factors have been implicated in the development of hypospadias, it has been widely accepted that hypospadias can be caused by impaired testosterone effects around the critical period for sex development (4). Furthermore, the mouse homolog is co-expressed with steroidogenic factor 1 (*SF1*; aliases, *AD4BP* and *NR5A1*) (3), which regulates the transcription of a vast array of genes involved in sex devel-

* This work was supported by Grant 17C-2 for Child Health and Development and Grant H18-005 for Research on Children and Families from the Ministry of Health, Labor, and Welfare and by Grants-in-aid 16086215 and 16590218 for Scientific Research on Priority Areas from the Ministry of Education, Science, Sports, and Culture. The costs of publication of this article were defrayed in part by the payment of page charges. This article must therefore be hereby marked "*advertisement*" in accordance with 18 U.S.C. Section 1734 solely to indicate this fact.

[S] The on-line version of this article (available at http://www.jbc.org) contains supplemental Fig. S1 and Table S1.

[1] To whom correspondence should be addressed: Dept. of Endocrinology and Metabolism, National Research Inst. for Child Health and Development, 2-10-1 Ohkura, Setagaya-ku, Tokyo 157-8535, Japan. Tel.: 81-3-3416-0181; Fax: 81-3-5494-7026; E-mail: mfukami@nch.go.jp.

[2] The abbreviations used are: CXorf6, chromosome X open reading frame 6; SF1, steroidogenic factor 1; MAML, mastermind-like; N-ICD, Notch intracellular domain; RBP-J, recombination signal binding protein-J; STAT, signal transducer and activator of transcription; siRNA, small interfering RNA; RFP, red fluorescent protein; GFP, green fluorescent protein; MLT, mouse Leydig tumor; hCG, human chorionic gonadotropin; CR, conserved region; EMSA, electrophoretic mobility shift assay; NMD, nonsense-mediated mRNA decay; RT, reverse transcriptase; CHX, cycloheximide; MAMLD1, mastermind-like domain-containing 1.

opment (5–7), suggesting a possible interaction between *SF1* and *CXorf6*.

Mastermind-like 2 (MAML2; alias, Mam-3) is a non-DNA-binding transcriptional co-activator in Notch signaling (8, 9) that plays an important role in cell differentiation in multiple tissues by exerting either inductive or inhibiting effects according to the context of the cells (10). Upon ligand-receptor interaction, Notch intracellular domain (N-ICD) is translocated from the cell surface to the nucleus and interacts with a DNA-binding transcription factor, recombination signal binding protein-J (RBP-J), to activate target genes like hairy/enhancer of split 1 (*Hes1*) and *Hes5* (11). In this canonical Notch signaling process, MAML2 forms a ternary complex with N-ICD and RBP-J at nuclear bodies, enhancing the transcription of the Notch target genes (8, 9, 12–14).

However, not all *Hes* genes are activated by the canonical Notch signaling pathway (11, 15, 16). Among such a distinct class of *Hes* genes, recent studies have shown that *Hes3* can be induced by stimulation with a Notch ligand, via a STAT3 (signal transducer and activator of transcription 3)-mediated pathway (17). This finding, together with the lack of *Hes3* induction by N-ICD (16), implies that *Hes3* represents a target gene of a noncanonical Notch signaling.

Here, we report that *CXorf6* produces a protein that has a structural homology with MAML2 and transactivates the *Hes3* promoter activity and that *CXorf6* is involved in testosterone production and harbors an *SF1* target sequence.

EXPERIMENTAL PROCEDURES

Structural Analysis of CXorf6 Protein—We searched BLAST and TBlastn data bases using the CXorf6 protein sequence (NP_005482) as a bait. Protein sequences for the CXorf6 orthologs were predicted by comparing the human CXorf6 sequence with the genomic and transcribed sequences of different organisms using Clustal_X (18). The unrooted phylogram was generated by Clustal_X (18) from the sequence alignment of CXorf6 proteins and was visualized using TreeView 1.6.6 (19).

Primers, Probes, and Small Interfering RNAs (siRNAs)—The sequences of primers, probes, and siRNAs utilized in this study are summarized in supplemental Table 1.

Plasmid Vectors Utilized for CXorf6 Analyses—The cDNAs of the full-length *CXorf6* (amino acids 1–701) and the minor splicing variant lacking exon 4 (ΔExon 4) were amplified from human fetal testis cDNA (Invitrogen) and subcloned into pEF-BOS vector (20) to construct the CXorf6 expression vector for the transactivation analysis. The expression vectors containing cDNAs of nonsense mutants and missense variants of *CXorf6* were constructed by mutagenesis. For the subcellular localization analysis, cDNAs for the wild-type, mutant, and variant *CXorf6* were designed to lose the start codon and fused to the C-terminal side of the gene encoding either red fluorescent protein (RFP) in pDsRED-monomer C1 vector or green fluorescent protein (GFP) in pAcGFP1-C1 vector (Clontech). For the Western blot analysis, cDNAs missing the start codon were subcloned into pCMV-Myc vector (Clontech).

We also utilized the following vectors reported in the literature: pEF-BOSneo-mNotch1 RAMIC with cDNA of mouse *N1-ICD* (21), pEF-BOSneo-aNotch2 with cDNA of mouse *N2-ICD* (22), pEF-BOS-Mam3 with cDNA of human *MAML2* (8), pHes1-luc with the promoter sequence of mouse *Hes1* (−467 ~ +46 bp), pHes5-luc with the promoter sequence of mouse *Hes5* (−800 ~ +73 bp), pHes3-luc with the promoter sequence of mouse *Hes3* (−2,715 ~ +261 bp) (16), pTP1-luc (pGa 981-6) with an iterated enhancer element with an RBP-J binding site (23), and pEF-BOS-Mam-3-GFP with *MAML2-GFP* fusion gene (8).

Cell Culture—We primarily utilized mouse Leydig tumor (MLT) cells (ATCC, CRL-2065™), which retain the capability to produce testosterone and the responsiveness to human chorionic gonadotropin (hCG) stimulation (24), because *CXorf6* is a causative gene for hypospadias that is predicted to result from impairment of hCG-dependent testosterone production around the critical period for sex development (4, 25) and because the mouse homolog for *CXorf6* is expressed in testosterone-producing Leydig cells (3). We also utilized COS1 cells and HEK293 cells depending on the experimental purposes. These cells were maintained in RPMI 1640 or Dulbecco's modified Eagle's medium supplemented with 10% fetal bovine serum.

Transactivation Analysis of CXorf6—Transactivation function of *CXorf6* was analyzed by the luciferase methods. MLT cells seeded in 6-well dishes ($1.0–1.5 \times 10^5$ cells/well) were transiently transfected using Lipofectamine 2000 (Invitrogen) with 0.6 μg of luciferase reporter vector, 0.6 μg of expression vector for *CXorf6* or *MAML2*, and/or 0.8 μg of expression vector for *N1-ICD* or *N2-ICD*, together with 20 ng of pRL-CMV vector used as an internal control. As controls for the expression vectors, empty counterpart vectors were transfected. Luciferase assays performed with a Lumat LB9507 (Berthold) at 48 h after transfection were repeated 4–5 times.

DNA Binding Analysis of CXorf6—We searched for conserved regions (CRs) between the mouse *Hes3* promoter sequence in the pHes3-luc vector and the human AL031847 sequence containing *HES3* and ~100.2 kb upstream and ~63.8 kb downstream regions using the BLAST data base and performed an electrophoretic mobility shift assay (EMSA) for the CRs using a Lightshift chemiluminescent EMSA kit (Pierce). The procedure was as described in the manufacturer's instructions. In short, MLT cells or COS1 cells cultured in a plate with a diameter of 10 cm were transfected with 5 μg of empty or human *CXorf6* cDNA positive vector, and nuclear extracts were obtained at 48 h after transfection. Then, a small amount of nuclear extracts was incubated with each of biotin-labeled 24–35-bp probes (20 fmol) covering the CRs, and the incubation mixture was subjected to gel electrophoresis. Subsequently, the biotin-labeled probe was detected by chemiluminescence on a nylon membrane.

Western Blot Analysis of CXorf6—Expression vectors for various Myc-tagged CXorf6 proteins (5 μg) were transfected into HEK293 cells in a plate with a diameter of 6 cm. Cell lysates obtained at 48 h after transfection were probed with antibodies for Myc and β-actin utilized as an internal control.

Subcellular Localization Analysis of CXorf6—Subcellular localization of CXorf6 proteins was studied by expressing fusion proteins with RFP or GFP. Vectors for fusion proteins (2

μg) were transfected into MLT cells in a glass dish with a diameter of 3.5 cm. The fluorescent signals were observed at 48–72 h after transfection using a laser-scanning microscope LSM510 (version 3.2; Carl Zeiss) shortly after nuclear staining with 4′,6-diamidino-2-phenylindole.

Nonsense-mediated mRNA Decay (NMD)—Reverse transcriptase (RT)-PCR was performed for two regions of *CXorf6* using lymphoblastoid cell lines of the patient with R653X and his heterozygous mother, with and without the treatment of an NMD inhibitor cycloheximide (CHX) (Sigma; 100 μg/ml, 8-h incubation) (26). The occurrence of NMD was assessed by the presence or absence of the PCR products on the agarose gel in the patient and by the heterozygosity or hemizygosity of the PCR products on the electrochromatograms (CEQ 8000 Autosequencer, Beckman Coulter) in the mother after demonstrating a random X-inactivation pattern by the previously described method (27). Furthermore, maternal RT-PCR products were subcloned with a TOPO TA cloning kit (Invitrogen); 100 clones were subjected to sequencing to confirm the stabilization of mRNA with a nonsense mutation after CHX treatment.

Expression Analysis of HES3/Hes3—Human cDNA samples of penile and genital skin fibroblasts were prepared by RT-PCR using tissues obtained, after receiving permission, from a prepubertal boy with phimosis and from a prepubertal patient with ambiguous genitalia and mutant androgen receptor gene. Other human cDNA samples were purchased from Invitrogen or Clontech. For mouse *Hes3*, RT-PCR was performed for the MLT cells.

Knockdown Analysis for Mouse CXorf6 Homolog—We performed transient knockdown assay for the mouse *CXorf6* homolog using two siRNAs (siRNA1 and siRNA2; final concentration 20 nM). The siRNAs were transfected into MLT cells seeded in 12-well dishes (5×10^4 cells in each well with 1 ml of culture medium, using Lipofectamine RNAimax (Invitrogen). A nontargeting RNA (4611G, Ambion) was similarly transfected as a negative control.

After 48 h of incubation, we the examined mRNA quantity of mouse *CXorf6* homolog in the harvested MLT cells and testosterone concentration in the culture medium using half of the wells. The relative amount of mRNA was determined by the Taqman real-time PCR method using the probe-primer mix for mouse *CXorf6* homolog (assay No. mm01293665_m1, ABI) on an ABI PRISM 7000, using β2-microglobulin for an endogenous control. Testosterone concentration was measured by an electrochemiluminescence immunoassay. In addition, we further analyzed the testosterone production potential of the siRNA-transfected MLT cells in the remaining wells. After changing the old medium with a fresh medium containing hCG (Mochida Pharmaceutical; final concentration, 50 IU/liter), we cultured the cells for a further 1 h and measured testosterone concentration in the medium. These siRNA experiments were performed three times.

SF1 Target Sequence in CXorf6—We searched for a putative SF1 binding site in the genomic sequences of *CXorf6* (AC109994) and the mouse homolog (NT_039706) and performed DNA binding and the transactivation analyses. For the DNA binding analysis, the ^{35}S-labeled 30-bp probes containing the putative SF1 binding site in *CXorf6* were incubated with nuclear extracts of COS1 cells transfected by an empty or human *SF1* cDNA positive vector (pRK5) (Addgene) or with recombinant mouse Sf1 protein and were subjected to gel electrophoresis. Similar analysis was also performed for a 32-bp probe harboring the known SF1 binding site of *CYP11A1* (28) as a control. Furthermore, the biotin-labeled 30-bp probes containing the wild-type or the mutated SF1 binding site were incubated with nuclear extracts of COS1 cells transfected by a human *SF1* cDNA positive vector (pCMX-PL2) and were subjected to gel electrophoresis.

For the transactivation analysis, a fragment (−1,924 ~ −1,690) containing a putative SF1 binding site of *CXorf6* was PCR-amplified and inserted into the pGL3 basic luciferase reporter vector (Promega). Furthermore, a reporter vector carrying the mutation in the putative SF1 binding site was generated by mutagenesis. These reporter vectors (0.5 μg) were transfected into the MLT cells together with the empty or human *SF1* cDNA positive expression vector (2.5 μg) as well as pRL-CMV vector (20 ng) used as an internal control. The luciferase assays were repeated three times.

Statistical Analysis—The results are expressed as the mean ± S.D. and statistical significance was determined by the *t* test. $p < 0.05$ was considered significant.

RESULTS

Structural Analysis of CXorf6 Protein—We found that CXorf6 protein has a unique structure with homology to that of MAML2 protein (Fig. 1*A*). A unique amino acid sequence, which we designated the mastermind-like (MAML) motif, was inferred from sequence alignment with MAML1, MAML2, and MAML3 proteins (8, 9). The MAML motif was well conserved among CXorf6 orthologs identified in frog, bird, and mammals (Fig. 1*B*). In addition, a serine-rich domain was identified in CXorf6, as well as glutamine- and proline-rich domains.

Transcriptional Transactivation by the Wild-type CXorf6 Protein—We examined whether the wild-type CXorf6 (with exon 4) protein is involved in Notch signaling (Fig. 2*A*). Expression of CXorf6 alone slightly but significantly increased the luciferase activity in the absence of *Hes* promoters (pGL2 basic only), probably via some backbone vector sequence. This phenomenon was more evident for other vectors such as pGL3 basic and pGL4 basic (not shown). Thus, we utilized pGL2 basic-based luciferase reporter constructs with the promoter sequences of *Hes1*, *Hes5*, and *Hes3* (16).

For the canonical Notch target genes *Hes1* and *Hes5* with the RBP-J binding site (16), CXorf6 was incapable of enhancing the promoter activities beyond those observed for the pGL2 basic only. MAML2 had no transactivating function, and N-ICDs activated the promoters. The N-ICD-induced promoter activities were further enhanced by CXorf6, probably because of additive or synergic effects via some backbone vector sequence, and by MAML2 because of its co-activator function. The results from the MAML2 and N-ICDs studies were consistent with those reported previously (8, 9, 16).

By contrast, for the noncanonical Notch target gene *Hes3* without the RBP-J binding site (16), CXorf6 alone was capable of enhancing its promoter activity, whereas MAML2 and

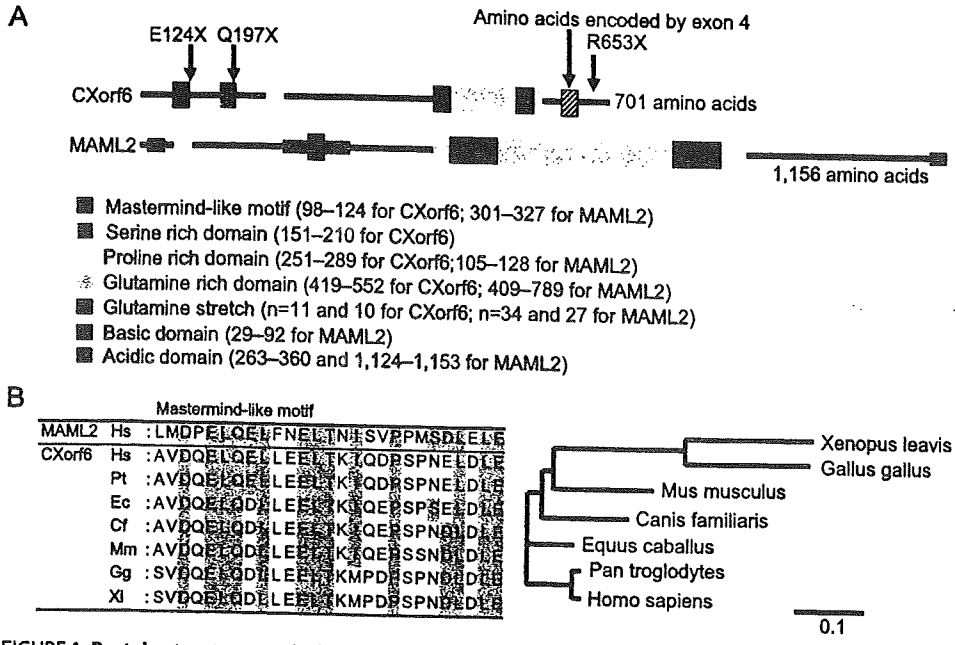

FIGURE 1. **Protein structure analysis.** *A*, the structure of human CXorf6 and MAML2 proteins. The identified domains are shown, together with the positions of the previously reported three nonsense mutations. *B*, amino acid sequence and a phylogenetic tree of the mastermind-like motif. *Hs*, *Homo sapiens* (human); *Pt*, *Pan troglodytes* (chimpanzee); *Ec*, *Equus caballus* (horse); *Cf*, *Canis familiaris* (dog); *Mm*, *Mus musculus* (mouse); *Gg*, *Gallus gallus* (chicken); *Xl*, *Xenopus laevis* (clawed frog). The conserved amino acids are *shaded*. In the phylogenetic tree, the horizontal distance indicates the degree of sequence divergence, and the *scale* represents the number of substitution events (10 per 100 amino acids).

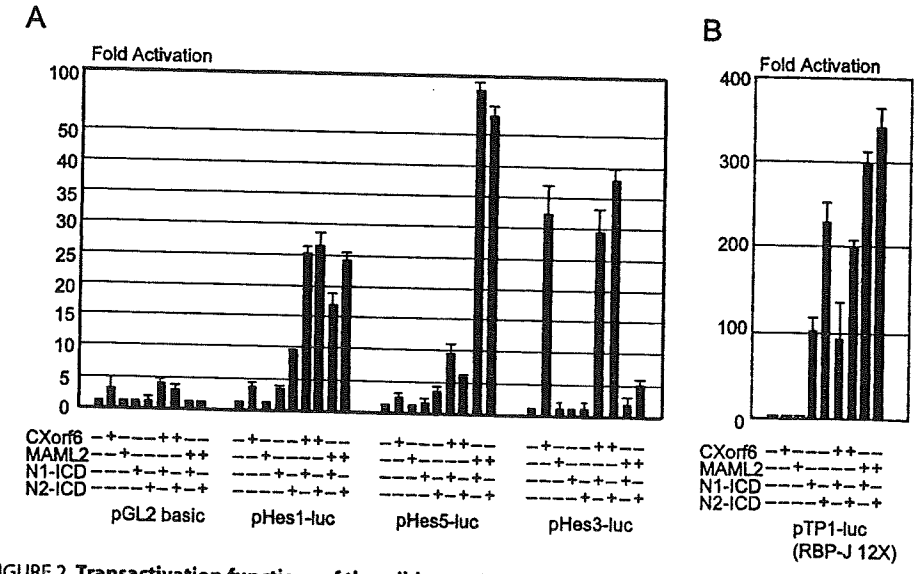

FIGURE 2. **Transactivation functions of the wild-type CXorf6 protein.** *A*, transactivating activities for pGL2 basic vector only and for pHes1-luc, pHes5-luc, and pHes3-luc vectors. The + symbols indicate the presence of expression vectors with cDNAs for *CXorf6*, *MAML2*, *N1-ICD*, and *N2-ICD*, and the − symbols denote the presence of expression vector only (*empty*). *B*, transactivating activities for pTP1-luc.

N-ICDs had no transactivating function. Consistent with this, co-expression of N-ICDs and CXorf6 or MAML2 exhibited no additive or synergic effects on the promoter activity.

These results argue that CXorf6 exerts its transactivation activity independently of the RBP-J binding sites. To confirm this, we performed similar analysis using pTP1-luc, which possesses an iterated enhancer element with an RBP-J binding site (23). As expected, CXorf6 was incapable of enhancing the N-ICD-induced transactivation, whereas MAML2 augmented the N-ICD-induced activities of this promoter (Fig. 2*B*).

DNA Binding Analysis of the Wild-type CXorf6 Protein—We attempted to examine whether the wild-type CXorf6 can bind to the *Hes3* promoter sequence directly (supplemental Fig. 1). Comparison of the 2,976-bp mouse *Hes3* promoter sequence with the human AL031847 sequence identified five CRs (CR1–CR5). Notably, the five CRs found in the human also resided in the upstream of the coding sequences of *HES3*, and the orientation of the CR1–CR5 was well conserved between human and mouse, whereas the mouse *Hes3* promoter region was associated with repeat sequences between CR4 and CR5. EMSA was carried out using 24–35-bp overlapping biotin-labeled probes covering the CR1–CR5 (total, 25 probes), showing no evidence for the DNA-binding capacity of CXorf6.

Transactivation Function of Mutant and Variant CXorf6 Proteins—We next analyzed the transactivating activities of the previously identified three apparently pathologic nonsense mutants and three apparently non-pathologic missense variants of *CXorf6* (3) (Fig. 3*A*) using the pHes3-luc vector. The E124X and Q197X proteins had no transactivation function, whereas the R653X protein as well as the three variant (P286S, Q507R, and N589S) proteins retained a nearly normal transactivating activity (Fig. 3*B*). In addition, the transactivation function was significantly reduced in the L103P protein (an artificially constructed variant affecting the MAML motif) and was normal in ΔExon 4. Transactivation analysis was also performed in the presence of N-ICDs, showing similar results (not shown). Western blot analysis for the three nonsense mutants verified the presence of proteins with expected molecular masses, whereas expression of the E124X protein appeared to be relatively reduced and that of Q197X protein was somewhat increased (Fig. 3*C*).

Subcellular Localization Analysis of Various CXorf6 Proteins—The RFP-CXorf6 (wild-type with exon 4) fusion protein were distributed in a speckled pattern and co-localized with the MAML2-GFP fusion protein (Fig. 4*A*). Furthermore, although the GFP-E124X and GFP-Q197X fusion proteins resided in the

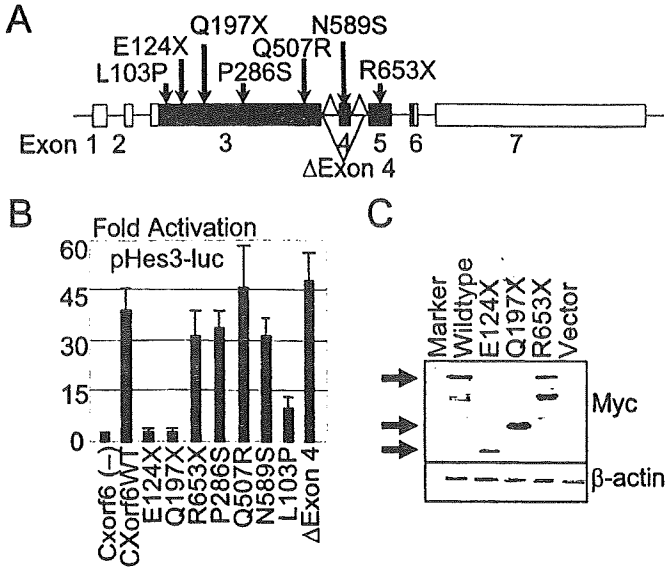

FIGURE 3. **Transactivation functions of the mutant and variant CXorf6 proteins.** *A*, the position of analyzed mutations and variations. L103P is an artificial substitution affecting the MAML motif, and the remaining mutations and variations are naturally occurring substitutions. ΔExon 4 is the minor splice variant lacking exon 4. The *black* and *white areas* denote the coding regions and the untranslated regions, respectively. *B*, transactivating activities of the mutant and variant CXorf6 proteins for the pHes3-luc in the absence of N-ICDs. *C*, Western blot analysis using antibodies for Myc and β-actin.

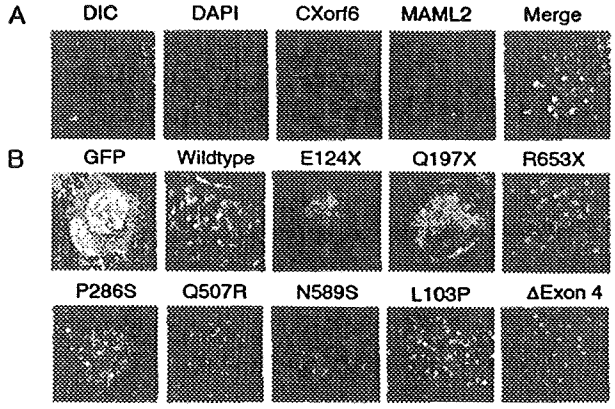

FIGURE 4. **Subcellular localizations of various CXorf6 proteins.** *A*, co-localization of the wild-type CXorf6 and MAML2 in nuclear bodies. Different images of a single cell are shown. The differential interference contrast (*DIC*) microscope image has been utilized for phase contrast, and nuclear counterstaining was performed with 4′,6-diamidino-2-phenylindole (*DAPI*). *B*, appearance of the mutant and the variant CXorf6 proteins after 4′,6-diamidino-2-phenylindole staining.

nucleus, they were incapable of localizing to the nuclear bodies (Fig. 4*B*). The remaining fusion proteins formed between the GFP and CXorf6 mutants and variants including R653X showed a punctate pattern (Fig. 4*B*) and co-localized with the RFP-CXorf6 (wild-type with exon 4) fusion protein (not shown).

Nonsense-mediated mRNA Decay—The above results indicate that the artificially produced R653X protein retains an almost normal function. In this regard, we have shown that R653X, as well as E124X and Q197X, causes NMD *in vivo*, by RT-PCR analysis of leukocytes of the patients (3). Indeed, the positions of these mutations including R653X (1957C > T) satisfy the condition for the occurrence of NMD (29).

To further confirm this event in the R653X mutation, we examined two regions of *CXorf6* mRNA obtained from lymphoblastoid cell lines of the patient and his heterozygous mother, using an NMD inhibitor, CHX (Fig. 5*A*). In the patient, RT-PCR amplification for regions 1 and 2 yielded no or very faint product without CHX treatment and a clear band with CHX treatment (Fig. 5*B*). In the mother, methylation pattern analysis of the androgen receptor gene (exon 1) indicated random X-inactivation (40:60%), and RT-PCR direct sequencing for a part of the region 2 encompassing the mutation delineated only the wild-type allele without CHX treatment and both wild-type and mutant alleles with CHX treatment (Fig. 5*C*). Furthermore, the analysis of 100 maternal RT-PCR clones showed only the wild-type sequence without CHX treatment and both wild-type and mutant sequences with a ratio of 56:44, which is similar to the X-inactivation ratio, after CHX treatment. These findings argue for the occurrence of NMD in the R653X mutation.

Expression Analysis of HES3/Hes3—PCR-based cDNA library screening for *HES3* identified variable degrees of expression in a range of tissues including fetal testis and adult ovary (Fig. 6). In addition, *Hes3* was expressed in the MLT cells (not shown).

Knockdown Analysis for Mouse CXorf6 Homolog—At 48 h after transfection, the mRNA level of the endogenous mouse *CXorf6* homolog was severely reduced in the MLT cells (relative amount: 28% for siRNA1 and 29% for siRNA2), indicating the successful knockdown (Fig. 7*A*). At that time, testosterone concentration was also significantly decreased in the medium harboring the knockdown cells (relative concentration: 63% for siRNA1 and 81% for siRNA2) (Fig. 7*B*). Furthermore, hCG-stimulated testosterone production during a subsequent 1 h was also compromised in the knockdown MLT cells (relative concentration: 53% for siRNA1 and 55% for siRNA2) (Fig. 7*C*).

SF1 Target Sequence in CXorf6—A putative SF1 binding sequence, CCAAGGTCA, was identified at intron 2 upstream of the coding region of *CXorf6* (−1,773 ~ −1,765) (Fig. 8*A*). This binding site was also found at intron 1 in the upstream coding region in the mouse homolog (−42,904 ~ −42,896 and −9,986 ~ −9,978) (not shown). Both human SF1 and mouse Sf1 proteins were capable of binding to the putative SF1 binding site of *CXorf6* as well as to the known SF1 binding site of *CYP11A1* (Fig. 8*B*). This SF1 protein binding was drastically reduced when the putative SF1 binding site CCAAGGTCA was mutated as CCATTGTCA (Fig. 8*C*). Consistent with this finding, although the SF1 protein transactivated the luciferase activity of the wild-type reporter, the transactivation function of SF1 protein was significantly reduced for the mutant reporter (Fig. 8*C*).

DISCUSSION

The wild-type CXorf6 co-localized with structurally related MAML2 in the nuclear bodies and transactivated the *Hes3* promoter without demonstrable DNA-binding capacity. These findings are consistent with transcription usually occurring around nuclear bodies (30, 31) and suggest that CXorf6 may be recruited to the *Hes3* promoter as a non-DNA-binding transcriptional co-activator, although the possibility that CXorf6

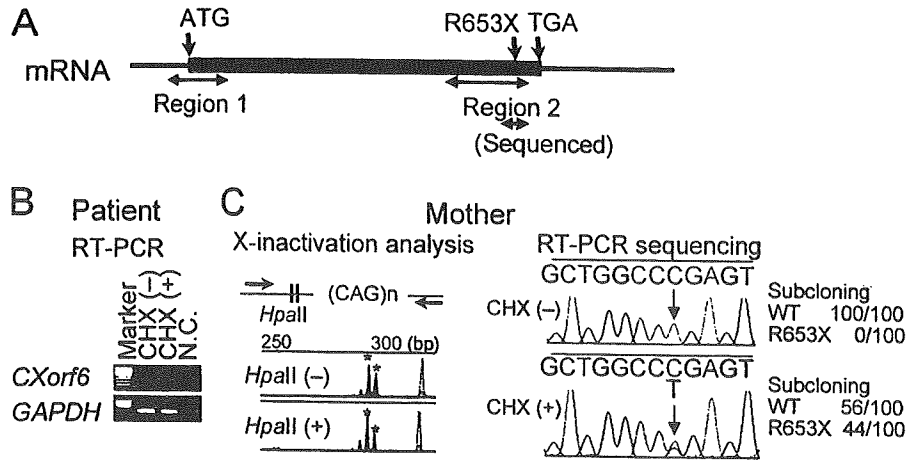

FIGURE 5. **The NMD analysis for the R653X mutation.** *A*, the position of the R653X mutation and the examined regions. Region 1 spans exon 2 to exon 3 and encompasses the start codon. Region 2 spans exon 3 to exon 5 and involves the mutation. The *gray regions* represent the coding region, and the *horizontal line* denotes the untranslated regions. *B*, representative results of the patient. After 40 cycles of RT-PCR for region 1, no band is seen without CHX treatment (CHX(−)), and a clear band is observed after CHX treatment (CHX(+)). *GAPDH*, glyceraldehyde-3-phosphate dehydrogenase gene; *N.C.*, negative control. *C*, representative results of the heterozygous mother. *Left*, X-inactivation analysis for a region encompassing the highly polymorphic CAG repeat tract and two methylation-sensitive HpaII sites at exon 1 of the androgen receptor gene. PCR products are obtained from both active and inactive X chromosomes before HpaII digestion and from inactive X chromosomes only after HpaII digestion. The comparison of the area under the curves between two heterozygous peaks (282 and 285 bp, marked with *asterisks*) before and after the HpaII digestion indicates that the two X chromosomes undergo random X-inactivation with a ratio of 40:60%. The small 276- and 279-bp peaks are byproducts of the slippage phenomenon. *Right*, RT-PCR direct sequencing for a region encompassing the mutation. The normal allele-only is delineated without CHX treatment (−), and the normal and nonsense alleles are identified with CHX treatment (+). The sequencing of 100 RT-PCR clones revealed wild-type clones-only (*WT*) without CHX treatment and both wild-type ($n = 56$) and mutant ($n = 44$) clones after CHX treatment.

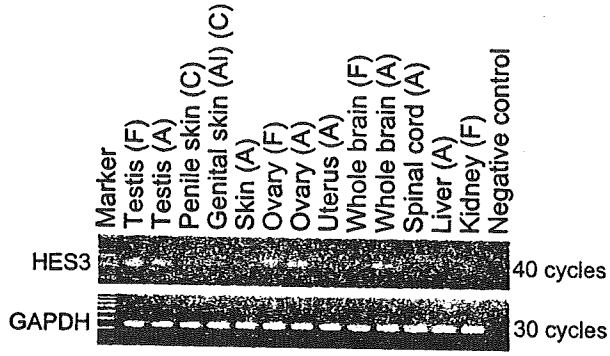

FIGURE 6. **PCR-based human cDNA screening for *HES3*.** The glyceraldehyde-3-phosphate dehydrogenase gene (*GAPDH*) was utilized as an internal control. *F*, fetus; *C*, child; *A*, adult; *AI*, androgen insensitivity.

protein can bind to a non-examined sequence(s) has not been excluded at present. It might be possible, therefore, that *MAML2* and *CXorf6* are distantly related molecules derived from a common ancestor and that *MAML2* has evolved as a co-activator for the RBP-J dependent canonical Notch signaling, whereas *CXorf6* has evolved as a co-activator for the transcription of noncanonical Notch target *Hes3*. In this regard, although MAML2 can augment the endogenous RBP-J-dependent transcription of canonical Notch target genes only in the presence of N-ICD (Refs. 8 and 9 and the present study), CXorf6 alone was capable of enhancing the *Hes3* promoter activity. This would be relevant to CXorf6 being devoid of the N-terminal region of MAML2 including the basic domain, which is essential for the ternary complex formation of MAML2 with N-ICD and RBP-J at the nuclear bodies (8, 9, 12–14), and implies that CXorf6 may directly interact with an unknown endogenous DNA-binding transcription factor for *Hes3*. Although STAT3 may be a candidate DNA-binding transcription factor for *Hes3* (17), there have been no data indicating a STAT3 binding to the *Hes3* promoter in the noncanonical Notch signaling pathway, and *STAT3* is expressed predominantly in the germ cells rather than in the *CXorf6* expression positive Sertoli and Leydig cells in the developing testis (32). Thus, further studies are required to clarify how *CXorf6* transactivates *Hes3* transcription. In addition, there may be other target gene(s) of *CXorf6* besides *Hes3*.

Several domains were identified in the CXorf6 protein in addition to the previously reported glutamine- and proline-rich domains (1). In this regard, the evolutionally conserved MAML motif may play a critical role in the transactivating activity, because the L103P protein had a reduced transactivation function. The serine-rich domain may also be relevant to the transactivation (33). Furthermore, it is inferred that a nuclear localization signal resides on the N-terminal 123 amino acids and a nuclear body localization signal lies on amino acids 197–653, except for amino acids 567–607 encoded by exon 4. It might be possible that a nuclear body localization signal is preserved in the Q197X protein, and in the E124X protein as well, but could not function because of an aberrant protein folding.

Functional studies provided the molecular basis for the previously identified mutations and variations. The E124X and Q197X mutations previously have been shown to undergo NMD (3); if a small amount of truncated proteins were produced by mRNAs escaping NMD, such proteins would be nonfunctional. For the R653X mutation, although the artificially produced truncated protein had a normal transactivation function *in vitro*, the NMD analysis implies the occurrence of nearly complete NMD *in vivo*. The P286S, Q507R, and N589S proteins were confirmed to retain normal functions. These results are consistent with the previous genotype-phenotype correlations of the mutations and variations (3).

The siRNA experiments imply that *CXorf6* is involved in testosterone production. In this context, it appears that testosterone production is not abolished in the absence of residual *CXorf6* expression, because the degree of reduction was more obvious for the mRNA level than for the testosterone concentration. This would be consistent with the development of hypospadias in patients with *CXorf6* nonsense mutations (3), because hypospadias is a phenotype caused by reduced, but not absent, testosterone effects around the critical period for sex development (4, 25). When testosterone effects are abolished,

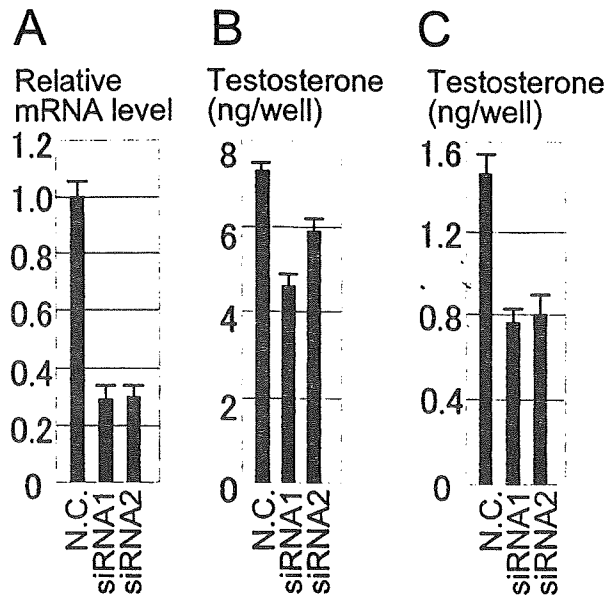

FIGURE 7. **Effects of siRNA on testosterone production in the MLT cells.** *A*, relative mouse *CXorf6* mRNA level in MLT cells after 48 h of incubation with two siRNAs. *B*, testosterone concentration in the medium after 48 h of incubation with two siRNAs. *C*, testosterone concentration in the medium after one h of incubation with hCG, using MLT cells cultured with two siRNA for 48 h. *N.C.*, negative control transfected with nontargeting RNA.

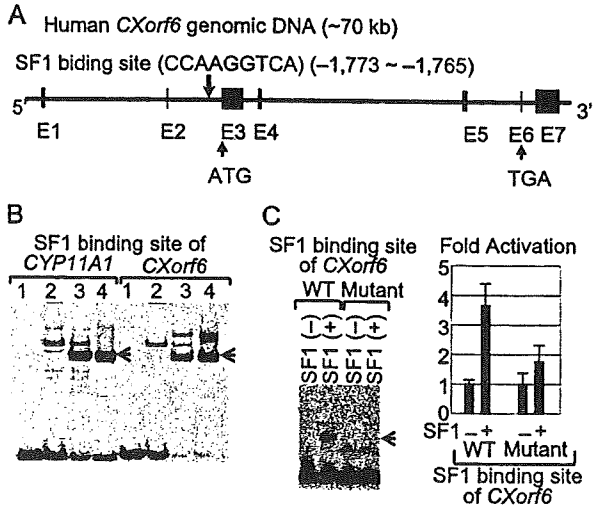

FIGURE 8. **Interaction between *SF1* and *CXorf6*.** *A*, genomic sequence of *CXorf6*. The putative SF1 binding site is present at intron 2 in the upstream of the coding region. The *black areas* indicate exons E1–E7, with the start codon (ATG) on exon 3 and the stop codon (TGA) on exon 6. *B*, EMSA using the ^{35}S-labeled probes containing the previously known SF1 binding site of *CYP11A1* and the putative SF1 binding site of *CXorf6*. *Lane 1*, probe only; *lane 2*, mixture of the probe and nuclear extract of COS1 cells transfected with an empty vector; *lane 3*, mixture of the probe and nuclear extract of COS1 cells transfected with an expression vector with human *SF1* cDNA; *lane 4*, mixture of the probe and recombinant mouse Sf1 protein. *Arrows* indicate the bands retarded due to the binding of the SF1/Sf1 protein. *C*, EMSA and transactivation analysis using wild-type (*WT*) and mutant sequences for the putative SF1 binding site. The binding of SF1 protein to biotin-labeled probes is drastically reduced for the mutant probe (shown by an *arrow*), and the relative luciferase activity is obviously decreased for the reporter with the mutant sequence.

this results in female external genitalia in genetic males (25). Thus, it is likely that *CXorf6* augments testosterone production.

The present study has implications for the molecular network involving *CXorf6*. *HES3* was expressed in the human fetal testis, and the *Hes3* promoter was transactivated by *CXorf6*. *Sf1* is co-expressed with the mouse homolog for *CXorf6* in fetal Sertoli cells and Leydig cells (3), and SF1 transactivated *CXorf6*. Thus, there may be an interaction among *SF1*, *CXorf6*, and *HES3* in the fetal testis, which may play an important role in the testicular function including testosterone production. In this regard, although the mouse homolog for *CXorf6* is not expressed in the adult testis, it is clearly expressed in the adult ovary (3) where *SF1* (4, 5) and *HES3* are also expressed. In addition, premature ovarian failure has been described in a female with heterozygosity for a microdeletion involving *CXorf6* (34). Thus, *CXorf6* and its possible interaction with *SF1* and *HES3* may also be relevant to adult ovarian function.

In summary, the present study implies that *CXorf6* transactivates the *Hes3* promoter, augments testosterone production, and contains the *SF1* target sequence, thereby providing the first clue for the elucidation of the *CXorf6* function. On the basis of the characteristic structure, we have therefore designated *CXorf6* as *MAMLD1*.

Acknowledgments—The reporter vectors pHes1-luc, pHes5-luc, and pHes3-luc were kindly provided by Prof. R. Kageyama, the pEF-BOS-neo-mNotch1 RAMIC vector by Prof. T. Honjo, pEF-BOSneo-aNotch2 by Prof. S. Chiba, pEF-BOS vector by Prof. S. Nagata, Mam-3 cDNA (MAML2, KIAA1819) by Prof. T. Nagase, and pTP1-luc vector by Dr. L. Strobl. We also thank Drs. S. Ikegawa and K. Miyado for technical assistance.

REFERENCES

1. Laporte, J., Kioschis, P., Hu, L. J., Kretz, C., Carlsson, B., Poustka, A., Mandel, J. L., and Dahl, N. (1997) *Genomics* **41**, 458–462
2. Hu, L. J., Laporte, J., Kress, W., Kioschis, P., Siebenhaar, R., Poustka, A., Fardeau, M., Metzenberg, A., Janssen, E. A., Thomas, N., Mandel, J. L., and Dahl, N. (1996) *Hum. Mol. Genet.* **5**, 139–143
3. Fukami, M., Wada, Y., Miyabayashi, K., Nishino, I., Hasegawa, T., Nordenskjöld, A., Camerino, G., Kretz, C., Buj-Bello, A., Laporte, J., Yamada, G., Morohashi, K., and Ogata, T. (2006) *Nat. Genet.* **38**, 1369–1371
4. Baskin, L. S., and Ebbers, M. B. (2007) *J. Pediatr. Surg.* **41**, 463–472
5. Morohashi, K., and Omura, T. (1996) *FASEB J.* **10**, 1569–1577
6. Parker, K. L., and Schimmer, B. P. (1997) *Endocr. Rev.* **18**, 361–377
7. Ozisik, G., Achermann, J.C., and Jameson, J. L. (2002) *Mol. Genet. Metab.* **76**, 85–91
8. Lin, S. E., Oyama, T., Nagase, T., Harigaya, K., and Kitagawa, M. (2002) *J. Biol. Chem.* **277**, 50612–50620
9. Wu, L., Sun, T., Kobayashi, K., Gao, P., and Griffin, J. D. (2002) *Mol. Cell. Biol.* **22**, 7688–7700
10. Artavanis-Tsakonas, S., Rand, M. D., and Lake, R. J. (1999) *Science* **284**, 770–776
11. Iso, T., Kedes, L., and Hamamori, Y. (2003) *J. Cell. Physiol.* **194**, 237–255
12. Tonon, G., Modi, S., Wu, L., Kubo, A., Coxon, A. B., Komiya, T., O'Neil, K., Stover, K., El-Naggar, A., Griffin, J. D., Kirsch, I. R., and Kaye, F. J. (2003) *Nat. Genet.* **33**, 208–213
13. Nam, Y., Sliz, P., Song, L., Aster, J. C., and Blacklow, S. C. (2006) *Cell* **124**, 973–983
14. Wilson, J. J., and Kovall, R. A. (2006) *Cell* **124**, 985–996
15. Sasai, Y., Kageyama, R., Tagawa, Y., Shigemoto, R., and Nakanishi, S. (1992) *Genes Dev.* **6**, 2620–2634
16. Nishimura, M., Isaka, F., Ishibashi, M., Tomita, K., Tsuda, H., Nakanishi, S., and Kageyama, R. (1998) *Genomics* **49**, 69–75
17. Androutsellis-Theotokis, A., Leker, R. R., Soldner, F., Hoeppner, D. J., Ravin, R., Poser, S. W., Rueger, M. A., Bae, S. K., Kittappa, R., and McKay, R. D. (2006) *Nature* **442**, 823–826
18. Thompson, J. D., Gibson, T. J., Plewniak, F., Jeanmougin, F., and Higgins, D. G. (1997) *Nucleic Acids Res.* **25**, 4876–4882

19. Page, R. D. (1996) *Comput. Appl. Biosci.* **12,** 357–358
20. Mizushima, S., and Nagata, S. (1990) *Nucleic Acids Res.* **18,** 5322
21. Mizutani, T., Taniguchi, Y., Aoki, T., Hashimoto, N., and Honjo, T. (2001) *Proc. Natl. Acad. Sci. U. S. A.* **98,** 9026–9031
22. Shimizu, K., Chiba, S., Saito, T., Kumano, K., Hamada, Y., and Hirai, H. (2002) *Biochem. Biophys. Res. Commun.* **291,** 775–779
23. Minoguchi, S., Taniguchi, Y., Kato, H., Okazaki, T., Strobl, L. J., Zimber-Strobl, U., Bornkamm, G. W., and Honjo, T. (1997) *Mol. Cell. Biol.* **17,** 2679–2687
24. Panesar, N. S., Chan, K. W., and Ho, C. S. (2003) *Steroids* **68,** 245–251
25. Grumbach, M. M., Hughes, I. A., and Conte, F. A. (2002) in *Williams Textbook of Endocrinology* (Larsen, P. R., Kronenberg, H. M., Melmed, S., and Polonsky, K. S., eds) 10th Ed., pp. 842–962, Saunders, Philadelphia
26. Freddi, S., Savarirayan, R., and Bateman, J. F. (2000) *Am. J. Med. Genet.* **90,** 398–406
27. Muroya, K., Kosho, T., Matsuo, M., and Ogata, T. (1999) *Am. J. Med. Genet.* **84,** 384–385
28. Liu, Z., and Simpson, E. R. (1997) *Mol. Endocrinol.* **11,** 127–137
29. Kuzmiak, H. A., and Maquat, L. E. (2006) *Trends Mol. Med.* **12,** 306–316
30. Zhong, S., Salomoni, P., and Pandolfi, P. P. (2000) *Nat. Cell Biol.* **2,** E85–E90
31. Wu, L., Aster, J. C., Blacklow, S. C., Lake, R., Artavanis-Tsakonas, S., and Griffin, J. D. (2000) *Nat. Genet.* **26,** 484–489
32. Murphy, K., Carvajal, L., Medico, L., and Pepling, M. (2005) *Gene Expr. Patterns* **5,** 475–482
33. Nowling, T. K., Johnson, L. R., Wiebe, M. S., and Rizzino, A. (2000) *J. Biol. Chem.* **275,** 3810–3818
34. Bartsch, O., Kress, W., Wagner, A., and Seemanova, E. (1999) *Cytogenet. Cell Genet.* **85,** 310–314

Doi: 10.1111/j.1742-7843.2008.00309.x
 Basic & Clinical Pharmacology & Toxicology, 103, 468–475

Omeprazole Alleviates Benzo[a]pyrene Cytotoxicity by Inhibition of CYP1A1 Activity in Human and Mouse Hepatoma Cells

Kazuhiro Shiizaki[1], Seiichiroh Ohsako[2], Masanobu Kawanishi[1] and Takashi Yagi[1]

[1]Environmental Genetics Laboratory, Frontier Science Innovation Center, Osaka Prefecture University, Osaka, Japan, and
[2]Division of Environmental Health Sciences, Center for Disease Biology and Integrated Medicine, Graduate School of Medicine, University of Tokyo, Tokyo, Japan

(Received March 27, 2008; Accepted June 2, 2008)

Abstract: Omeprazole is a drug used for treating gastro-oesophageal reflux disease and duodenal ulcers. Omeprazole induces a xenobiotic-metabolizing enzyme, cytochrome P450 1A1 (CYP1A1), as its ligand by aryl hydrocarbon receptor (AhR) activation without binding. CYP1A1-inducible chemicals, such as benzo[a]pyrene and 2,3,7,8-tetrachlorodibenzo-*p*-dioxin, are known to have adverse effects (i.e. carcinogenesis, mutagenesis and malformation). Unlike these typical AhR activators, omeprazole has shown no experimental evidence of carcinogenic activity. The possibility, however, remains that omeprazole may aggravate the effect of environmental carcinogens through CYP1A1 induction. We exposed benzo[a]pyrene and omeprazole simultaneously to human and mouse hepatoma cells to investigate the synergistic effect of these chemicals. Contrary to our prediction, cytotoxicity of benzo[a]pyrene was inhibited by the omeprazole exposure in a dose-dependent manner. Omeprazole did not alter CYP1A1 mRNA and protein levels induced by benzo[a]pyrene. The 7-ethoxy-resorufin-O-deethylase assay revealed that omeprazole inhibited CYP1A1 enzyme activity. Kinetic analysis also demonstrated that it is a competitive inhibitor for CYP1A1. The K_m value of omeprazole against CYP1A1 activity was 50.1 μM. We conclude that the effects of omeprazole on CYP1A1 involve not only induction through AhR activation but also inhibition of its enzyme activity, and that the protective effect of omeprazole against benzo[a]pyrene cytotoxicity depends on the latter.

Omeprazole, a benzimidazole derivative, is a potent suppressor of gastric acid secretion [1] and has been used for treating gastro-oesophageal reflux disease and duodenal ulcers. Omeprazole is known to have two distinct effects on drug metabolic enzymes: as an inhibitor of cytochrome P450 2C19 (CYP2C19) and as an inducer of CYP1A1 [2,3], and it also shows adverse abilities of both induction and inhibition against CYP3A4 [4].

CYP1A1 is known as a xenobiotic-metabolizing enzyme, and its transcriptional activation is mediated by aryl hydrocarbon receptor (AhR) [5,6]. AhR is identified as a ligand-activated transcription factor and member of the basic helix–loop–helix super family protein. Following the binding to ligands, such as 2,3,7,8-tetrachlorodibenzo-*p*-dioxin, AhR translocates to the nucleus and forms a heterodimer with AhR nuclear translocator [7]. The AhR/AhR nuclear translocator complex enhances the transcription of genes for phase I drug-metabolizing enzymes, including CYP1A1, 1A2 and 1B1 [8]. As AhR ligands such as benzo[a]pyrene are metabolized by CYP1A1, one of the functions of AhR is presumed to be that of a sensor for environmental chemicals or drugs [9].

Interestingly, unlike the typical AhR activator, omeprazole induces CYP1A1 without binding to AhR as a ligand [10]. Because CYP1A1 induction by omeprazole requires AhR, omeprazole has been thought to activate AhR through a different pathway from ligand binding [11]. The omeprazole-mediated AhR activation is reported to be species-specific. CYP1A1 induction by omeprazole has been shown in primary hepatocytes or hepatoma cell lines of man but not of mouse [12]. The omeprazole-mediated CYP1A1 induction requires more than 12 hr after the omeprazole treatment, which is slower compared to the benzo[a]pyrene-mediated induction [13]. Some reports suggest that protein phosphorylation is correlated to the omeprazole-mediated AhR activation, because some protein kinase inhibitors can block the activation [14,15]. However, the molecular mechanisms of omeprazole-mediated AhR activation are still unclear.

Some CYP1A1-inducible chemicals are known to produce adverse effects, such as carcinogenesis, mutagenesis and malformation. Among these chemicals, benzo[a]pyrene binds to the aryl hydrocarbon receptor as a ligand and induces CYP1A1 expression [16]. Subsequently, it is metabolized by CYP1A1 to electrophilic species, such as benzo[a]pyrene-7,8-dihydrodiol-9,10-epoxide, which can eventually produce bulky DNA adducts or oxidative DNA damage [17]. In addition, benzo[a]pyrene and other polyaromatic hydrocarbons have been shown to induce apoptosis in Hepa-1c1c7 cells [18]. CYP1A1 induction plays a key role in these toxic events, because CYP1A1- or AhR-deficient sub-lines derived from Hepa-1c1c7 cells show resistance against benzo[a]pyrene exposure [19].

Author for correspondence: Takashi Yagi, Environmental Genetics Laboratory, Frontier Science Innovation Center, Osaka Prefecture University, 1-2 Gakuen-cho, Naka-ku, Sakai-city, Osaka 599-8570, Japan (fax +81-072-254-9938, e-mail yagi-t@riast.osakafu-u.ac.jp).

Although omeprazole is an AhR activator, no experimental evidence about its carcinogenic activity and metabolic activation has been reported [20]. Omeprazole, when administered at the clinical level, does not cause toxicity through AhR activation [21]. The possibility that omeprazole aggravates the effect of precarcinogens through CYP1A1 induction, however, still remains.

In this study, we exposed human and mouse hepatoma cells to benzo[a]pyrene and omeprazole simultaneously to examine the synergistic effect of these chemicals. Unexpectedly, we found that cytotoxicity of benzo[a]pyrene is alleviated by omeprazole exposure. We demonstrate that CYP1A1 induction through AhR activation and inhibition of CYP1A1 activity are significant effects of omeprazole in benzo[a]pyrene-treated cells.

Materials and Methods

Cell culture. Mouse hepatoma Hepa-1c1c7 and human hepatoma HepG2 cells were obtained from American Type Culture Collection (Rockville, MD, USA). The cells were grown with Dulbecco's modified Eagle's medium (Invitrogen, Carlsbad, CA, USA) containing 10% foetal bovine serum and antibiotics (Invitrogen). Cell cultures were carried out under standard ambient conditions at 37° and 5% CO_2.

Chemicals. Omeprazole, ethoxy-resorufin, ellipticine and ketoconazole were purchased from Sigma (St. Louis, MO, USA). Benzo[a]pyrene was obtained from Wako Pure Chemical (Osaka, Japan). Neutral red was obtained from Nacalai Tesque (Kyoto, Japan). Benzo[a]pyrene was dissolved in acetone and other compounds were dissolved in dimethyl sulfoxide. All the compounds were added to cultured cells to obtain a solvent with a final concentration of 0.1%.

Neutral red uptake assay. Cells were incubated on 48-well tissue culture plates at a concentration of 0.5×10^4 cells in 200 µl per well. After benzo[a]pyrene exposure for 24 hr, the medium was replaced by fresh medium containing 50 µg/ml neutral red. After incubation for another hour, the medium was removed. The cells were carefully washed twice with phosphate-buffered saline (PBS), and the neutral red incorporated into the cells was extracted with 100 µl of ethanol containing 1% acetic acid. Neutral red absorbance value at a wavelength of 570 nm was measured with the Model 550 microplate reader (Bio-Rad, Hercules, CA, USA).

Real-time reverse transcription–polymerase chain reaction analysis. Cells plated in 6-well plates at 80% confluence were exposed to a combination of omeprazole and benzo[a]pyrene. After 8 hr of exposure, total RNA was isolated using Isogen (Nippon Gene, Tokyo, Japan) according to the manufacturer's instructions. An aliquot (2 µg) of total RNA was subjected to reverse transcription in a 40-µl reaction mixture containing 0.5 mM dNTP (dATP, dCTP, dGTP, and dTTP), 25 U reverse transcriptase (MultiScribe; Applied Biosystems, Foster City, CA, USA), 2.5 µM oligo (dT) primers, 1× reverse transcriptase buffer and 5.5 mM $MgCl_2$. The reaction mixture was incubated with stepwise increases in temperature at 25° for 10 min., 48° for 40 min., and 95° for 5 min.

For mouse and human CYP1A1 mRNA quantification, real-time polymerase chain reaction (PCR) was performed by using the LightCycler instrument (Roche, Manheim, Germany). A primer pair for the mouse CYP1A1 cDNA amplification was as follows: forward primer, 5′-TAAAACACGCCCGCTGTGAA-3′; reverse primer, 5′-AAGTAGGAGGCAGGCACAATGTC-3′. A primer pair for the human CYP1A1 cDNA amplification was as follows: forward primer, 5′-CATAGACACTGATCTGGCTGCAG-3′; reverse primer, 5′-GGGAAGGCTCCATCAGCATC-3′. The human and mouse CYP1A1 cDNA fragments were amplified by Taq DNA polymerase (Gene Taq; Nippon Gene) with the primers described above and then inserted into a pGEM-T easy vector individually. The molecular weight of each plasmid DNA was calculated and its stock solution was diluted from 2×10^7 to 2×10^3 copies/µl for generating the calibrator DNA. An aliquot of the cDNA (2 µl) or calibrator plasmid DNA was amplified along with a master mixture (Fast-Start SYBR Green I kit; Roche) containing the CYP1A1-specific primers described above at a final volume of 20 µl. The reaction mixture was amplified under the following cycle condition: an initial incubation of 95° for 15 min. followed by 40 cycles of 95° for 15 sec., 60° for 20 sec., and 72° for 10 sec. The fluorescent products were detected at the end of the 72° extension period. To confirm amplification specificity, the PCR products were subjected to a melting curve analysis. The calibration curve was generated by threshold cycles of calibrators with a known copy number. The starting quantity of CYP1A1 mRNA in the samples was determined from correlation of their threshold cycles to the calibration curve.

Western blot analysis. CYP1A1 protein was detected by immunoblot analysis using polyclonal antibody against human CYP1A1 (Daiichi Pure Chemicals, Tokyo, Japan). Cells were plated on a 6-well plate at a density of 4×10^4 cells per well. After 16 hr of benzo[a]pyrene (1.25 µg/ml) and/or omeprazole (50 and 100 µM) treatment, the cells were lysed with 500 µl of sodium dodecyl sulfate (SDS) sample buffer (62.5 mM Tris-HCl, pH 7.4, 2% SDS). The total cell lysates were sonicated on ice in a 1.5-ml microcentrifuge tube for 30 sec. and then centrifuged at 20,000 ×g for 10 min. at 4°. Protein concentration of each sample was determined by the Bradford dye-binding method (Protein assay; Bio-Rad). An aliquot of 20 µg of protein was denatured by adding 2-mercaptoethanol (final concentration 5%) and heated at 95° for 3 min. The samples were allowed to cool to room temperature, and denatured samples were separated on a denaturing polyacrylamide gradient-buffered gel (ExelGel SDS Homogenous 7.5; GE Healthcare Biosciences, Tokyo, Japan) using Multiphor II Electrophoresis Unit (GE Healthcare Biosciences). The proteins were then electrophoretically transferred to nitrocellulose membranes. The membranes were soaked with blocking buffer (Block Ace; Daiichi Pure Chemicals) and probed with anti-rat CYP1A1 goat serum (Daiichi Pure Chemicals) or rabbit anti-actin polyclonal antibody (Sigma). The membranes were washed thoroughly with PBS containing 0.05% Tween-20. Antigen–antibody complexes were detected using horseradish peroxidase-conjugated anti-goat IgG (Chemicon International, Temecula, CA, USA) or anti-rabbit IgG (GE Healthcare Bioscience) with a chemiluminescence detection system (GE Healthcare Bioscience). For quantitative analysis, X-ray film was photographed by Printgraph (AE-6905H Image Saver; ATTO Bioinstrument, Tokyo, Japan), and the individual bands were quantified using a CS Analyser 2.0 system (ATTO Bioinstrument).

7-Ethoxy-resorufin-O-deethylase assay. 7-Ethoxy-resorufin-O-deethylase (EROD) assays were performed on intact living Hepa-1c1c7 cells as reported previously [22]. Cells were plated in 12-well plates (3×10^6 cells/well), allowed to grow to confluence, and treated with 1 µg/ml benzo[a]pyrene concomitantly with or without omeprazole (50 and 100 µM) in 500 µl of growth medium for 12 hr. Then, the medium was removed and the cells were washed with PBS. The assay was carried out by adding ethoxy-resorufin (final concentration, 5 mM) to the phenol red-free medium in the presence of newly added omeprazole with the same concentration of pre-treatment. The fluorescence of resorufin generated from the conversion of 7-ethoxy-resorufin by CYP1A1 was measured every 20 min. for 60 min. using a Labsystems Fluoroskan II fluorescence microplate reader (GMI Inc., Ramsey, MN, USA) with excitation at 544 nm and emission at 590 nm. A standard curve was constructed using resorufin. The EROD activity was expressed by quantification of resorufin as femtomole/10^{-5} cell/min.

Measurement of inhibition of human CYP activity by omeprazole. CYP activity was determined using P450-Glo CYP1A1 Assays, P450-Glo CYP3A4 Assays and P450-Glo CYP1A2 Assays (Promega, Madison, WI, USA) according to the manufacturer's instructions. The Sf9 cell microsomes containing recombinant human CYPs were purchased from Daiichi Pure Chemicals (Tokyo, Japan). An aliquot (0.5 μl) of microsomes was mixed with 100 mM KPO_4 buffer (25 μl) containing 120 μM of luciferin-6′-chloroethyl ether (CYP1A1), 120 μM of luciferin-6′-benzyl ether (CYP3A4) or 400 μM of luciferin-6′-methyl ether (CYP1A2). A 12.5-μl solution of omeprazole (0–500 μM) was added to each reaction cocktail and the mixtures were then incubated at 37° for 10 min. After preincubation, 25 μl of a 2× NADPH regenerating system solution (2.6 mM $NADP^+$, 6.6 mM glucose-6-phoshate, 0.4 unit/ml glucose-6-phoshate dehydrogenase and 6.6 mM $MgCl_2$) was added and the mixtures were incubated at 37° for 30 min. Luciferin converted from specific substrates by CYPs was detected by adding the Luciferin Detection Reagent included in the assay kit, and luminescence was determined in the Wallac Arvo SX Multi-Label counter (PerkinElmer, Boston, MA, USA). In order to determine IC_{50} values, activities were calculated with different omeprazole concentrations. Control activity was taken as 100% and the inhibitor concentrations causing 50% inhibition were determined from the graphs. In order to determine K_i constants with or without inhibitor, the assay was carried out with the various substrate (luciferin-6′-chloroethyl ether) concentrations (0.06, 0.12, 0.18, 0.24 and 0.30 mM), and the CYP1A1 activity was detected every 10 min. Lineweaver–Burk plots were drawn using 1/V versus 1/[S] values, and K_i constants were calculated from these graphs.

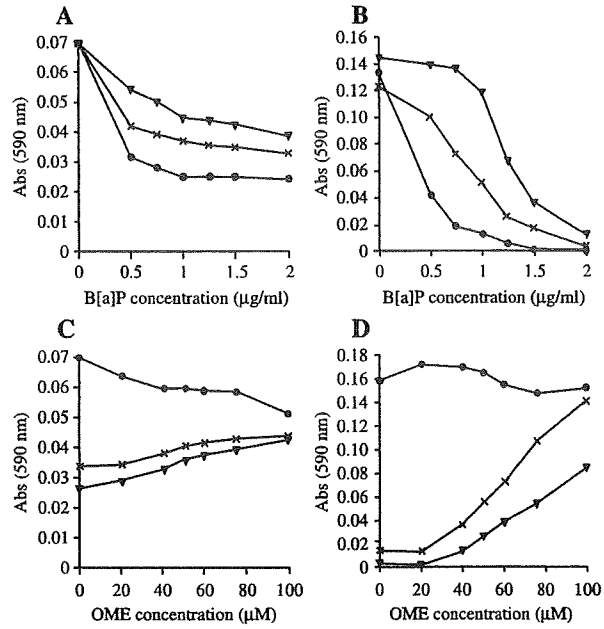

Fig. 1. Synergistic effects of omeprazole (OME) on benzo[a]pyrene (B[a]P)-induced cytotoxicity measured by neutral red uptake assay. HepG2 (A, C) and Hepa-1c1c7 cells (B, D) were plated in 48-well tissue culture plates. (A, B) Cells were exposed to a mixture of fixed concentration of OME (●, DMSO control; ×, 50 μM; ▼, 100 μM) with various concentrations (0–2 μg/ml)of B[a]P. (C, D) Cells were exposed to a mixture of fixed concentration of B[a]P (●, DMSO control; ×, 1 μg/ml; ▼, 1.5 μg/ml) with various concentrations of OME (0–100 μM). After 24 hr of exposure, the cell number was determined by neutral red uptake assay. The data points represent the mean of duplicate determinations. DMSO, dimethyl sulfoxide.

Results

Effect of omeprazole on benzo[a]pyrene toxicity in mouse and human hepatoma cells.

Omeprazole prevented the benzo[a]pyrene cytotoxicity in Hepa-1c1c7 and HepG2 cells in a dose-dependent manner as shown in fig. 1. This protection was more effective in Hepa-1c1c7 cells (fig. 1B and D) compared to HepG2 cells (fig. 1A and C). By the simultaneous exposure of omeprazole with variable doses of benzo[a]pyrene to Hepa-1c1c7 cells, cell death caused by the low-dose benzo[a]pyrene exposure (up to 0.75 mg/ml) was completely blocked by 100 μM omeprazole as shown in fig. 1B. Similar results were obtained in the experiment in which omeprazole was pre-treated 24 hr before benzo[a]pyrene exposure (data not shown).

Effect of omeprazole on benzo[a]pyrene-mediated CYP1A1 mRNA induction.

CYP1A1 mRNA was induced (18-fold compared to control) by the 50 μM omeprazole exposure alone in HepG2 cells (fig. 2A), while it was not induced in Hepa-1c1c7 cells (fig. 2C). Neither 10 μM nor 25 μM omeprazole exposure could induce CYP1A1 mRNA in HepG2 cells (data not shown). By exposure of benzo[a]pyrene (1 μg/ml), about 30-fold induction of CYP1A1 mRNA was obtained in Hepa-1c1c7 cells, and the induction was enhanced by dose-dependent addition of omeprazole (fig. 2D). In HepG2 cells, more than 200-fold induction of CYP1A1 mRNA was obtained by benzo[a]pyrene (1 μg/ml), and the induction was enhanced by adding 50 μM omeprazole but barely enhanced by adding 100 μM omeprazole (fig. 2B). These results suggest that the reduction of benzo[a]pyrene cytotoxicity by omeprazole observed in fig. 1 is not due to the inhibition of the transcriptional activation of CYP1A1.

Effect of omeprazole on CYP1A1 protein induction.

The CYP1A1 protein levels detected by Western blot analysis and quantitative analysis are shown in fig. 3. CYP1A1 protein could not be detected in Hepa-1c1c7 cells by dimethyl sulfoxide (control) or omeprazole treatment (fig. 3B). Weak bands were detected in HepG2 cells treated with 100 μM omeprazole (fig. 3A). In both cell lines, the CYP1A1 protein levels were significantly induced by benzo[a]pyrene exposure and were not altered by the addition of omeprazole. These results suggest that the alleviation of benzo[a]pyrene cytotoxicity by omeprazole observed in fig. 1 is not due to inhibition of CYP1A1 translation or the effects on the turnover of the CYP1A1 protein.

Effect of omeprazole on EROD activity.

The effect of omeprazole on the CYP1A1 activity was evaluated by the EROD assay (fig. 4). The EROD activity was significantly increased by benzo[a]pyrene exposure in both cell lines (fig. 4A versus B; fig. 4C versus D). The basal EROD activity was inhibited by the treatment with omeprazole alone in Hepa-1c1c cells (fig. 4C), but not in HepG2

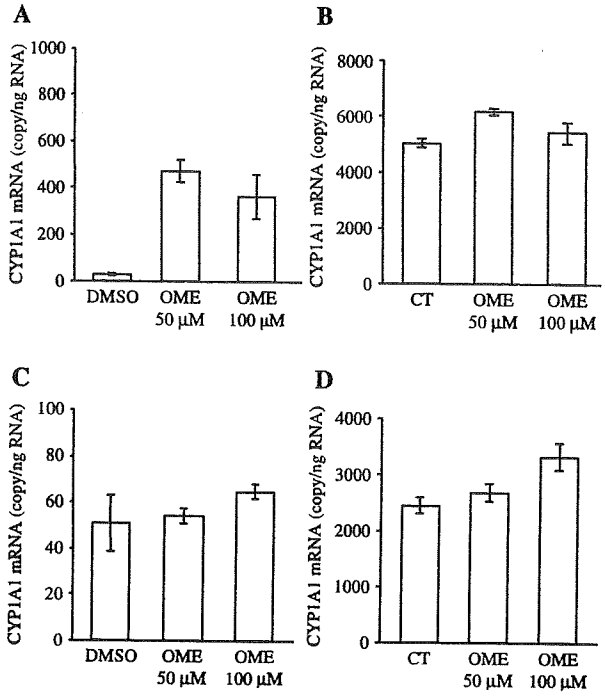

Fig. 2. Effects of omeprazole (OME) on CYP1A1 mRNA expression induced by benzo[a]pyrene (B[a]P). HepG2 cells (A, B) and Hepa-1c1c7 cells (C, D) were plated in 6-well tissue culture plates and exposed to OME (DMSO, 50 μM, 100 μM) concomitantly with (B, D: closed bar) or without 1 μg/ml of B[a]P (A, C: open bar). 'CT' represents control without OME but in the presence of B[a]P. After 8 hr of exposure, total RNA was isolated and human and mouse CYP1A1 mRNA were detected by real-time PCR. Data represent the value of CYP1A1 mRNA copy number in 1 ng total RNA. The mean of three independent experiments with S.D. is illustrated. DMSO, dimethyl sulfoxide.

cells (fig. 4A). Omeprazole decreased the benzo[a]pyrene-induced EROD activity in both Hepa-1c1c7 and HepG2 cells in a similar fashion (fig. 4B and D). The inhibition of the EROD activity was stronger in Hepa-1c1c7 cells compared to HepG2 cells. As the EROD activity reflects CYP1A1 and CYP1A2 activities [23], these results suggest that omeprazole alleviates benzo[a]pyrene cytotoxicity by the inhibition of one or both of these CYPs.

Determination of CYP species responsible for the protection of benzo[a]pyrene cytotoxicity.

Benzo[a]pyrene induces not only CYP1A1 but also CYP3A4 and CYP1A2, and these CYPs also metabolize and activate benzo[a]pyrene. It is also known that omeprazole has inhibitory activity of CYP3A4. Therefore, we examined the effects of ellipticine (CYP1A1/1A2 inhibitor) and ketoconazole (CYP3A4 inhibitor) on the cytotoxicity of the benzo[a]pyrene exposure to clarify which CYP dominantly contributes to cytotoxicity in Hepa-1c1c7 cells. As shown in fig. 5, ellipticine protected cytotoxicity (fig. 5A), while ketoconazole did not, at least in the tested doses (fig. 5B). The experiment could not be carried out with higher concentrations of the inhibitors because of their own cytotoxicity (data not shown). These

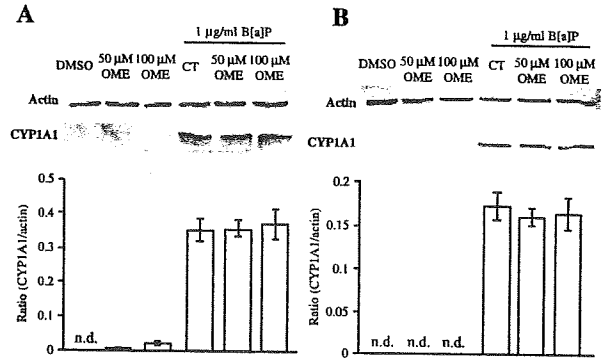

Fig. 3. Effects of omeprazole (OME) on CYP1A1 protein level induced by benzo[a]pyrene (B[a]P). HepG2 (A) or Hepa-1c1c7 cells (B) were plated in 6-well tissue culture plates and exposed to OME (DMSO, 50 μM, 100 μM) concomitantly with or without 1 μg/ml of B[a]P. 'CT' represents control without OME but in the presence of B[a]P. After 16 hr of exposure, cells were lysed with SDS sample buffer. The total cell lysates (20 μg protein) were analysed by Western blot for detecting CYP1A1 (lower panel) and actin (upper panel: internal control). The photographs shown are representatives of three independent experiments. The intensity of each band was quantified and the CYP1A1 protein level was normalized to the actin. Each column indicates the mean ± S.D. of the ratio of CYP1A1 protein to actin protein from three independent experiments. DMSO, dimethyl sulfoxide; n.d., not detected.

results suggest that CYP1A1 and CYP1A2 play a central role in the cytotoxicity induced by benzo[a]pyrene exposure.

Inhibition of recombinant human CYP activity by omeprazole.

The inhibition of CYP enzyme activity by omeprazole was measured with a specific substrate (fig. 6). CYP1A1 and CYP3A4 were inhibited by omeprazole in a dose-dependent manner, and IC_{50} values for the CYPs were 5.2 and 5.3 μM (fig. 6A and C, respectively). In contrast, omeprazole showed less inhibitory activity to CYP1A2 (IC_{50} > 100 μM) compared to CYP1A1 and CYP3A4 (fig. 6B). From the kinetic analysis shown in fig. 7, omeprazole was determined to be a competitive-type CYP1A1 inhibitor, because $1/V_{max}$ values, represented as the y-intercept, were almost the same with or without omeprazole (0.19 and 0.17) (fig. 7B). The K_i value of omeprazole against CYP1A1 activity was 3.21 μM and the K_m value of this enzyme was 50.1 μM.

Discussion

In the present study, to examine the possibility that omeprazole may aggravate the effect of environmental carcinogens through CYP1A1 induction, we exposed benzo[a]pyrene and omeprazole simultaneously to human and mouse hepatoma cells. Omeprazole-induced CYP1A1 induction has been reported to be species-specific, and it induces CYP1A1 through AhR activation in human cells, but not in mouse cells and tissues [12]. Therefore, it is expected that it does not affect benzo[a]pyrene cytotoxicity in mouse Hepa-1c1c7 cells, because the expression of CYP1A1 mRNA was barely

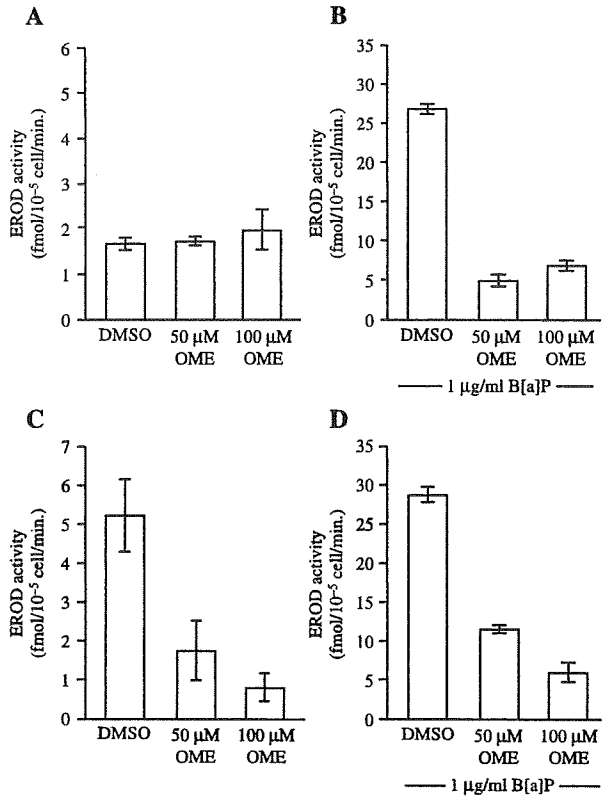

Fig. 4. Effects of omeprazole (OME) on EROD activity induced by benzo[a]pyrene (B[a]P). HepG2 (A, B) or Hepa-1c1c7 cells (C, D) were treated with OME (DMSO, 50, 100 μM) concomitantly with (B, D) or without (A, C) 1 μg/ml B[a]P for 12 hr. EROD activity was determined by adding 5 mM ethoxy-resorufin to the medium. The generated resorufin was measured after 60 min. of incubation by fluorescence plate reader with excitation at 544 nm and emission at 590 nm. Results represent the average of three independent experiments (mean ± S.D.). Note that the scales of the *x*-axis are different. DMSO, dimethyl sulfoxide.

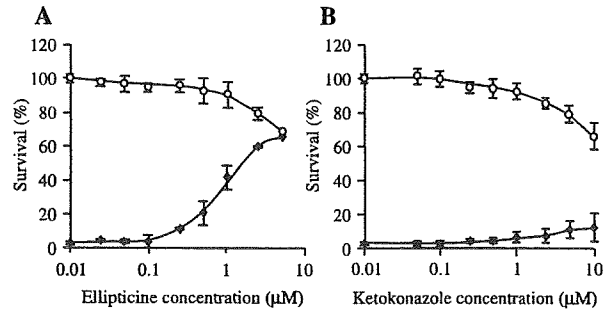

Fig. 5. Protective effects of CYP inhibitors on benzo[a]pyrene (B[a]P)-induced cytotoxicity in Hepa-1c1c7. (A) Cells were plated in a 48-well tissue culture plate and exposed to 0.01–3 μM ellipticine concomitantly with (◆) or without (○) 1 μg/ml of B[a]P. (B) Cells were exposed to 0.01–3 μM ketoconazole concomitantly with (◆) or without (○) 1 μg/ml B[a]P. After 24 hr of exposure, cell number was determined by neutral red uptake assay, and survival ratio was calculated by using absorbance of solvent control as 100%. Results represent the average of values from triplicate determinations (mean ± S.D.).

induced (fig. 2C). Omeprazole induced CYP1A1 mRNA only in human HepG2 cells (fig. 2A). Contrary to expectation, omeprazole reduced benzo[a]pyrene cytotoxicity in both mouse and human cells in a similar fashion (fig. 1). These results suggest that the CYP1A1 induction by omeprazole could be irrelevant to the aggravation of benzo[a]pyrene cytotoxicity.

The cytotoxicity of benzo[a]pyrene requires metabolic activation by specific CYPs, because it is not reactive *per se*. If benzo[a]pyrene metabolites such as benzo[a]pyrene-7,8-dihydrodiol-9,10-epoxide were produced by CYPs, they form DNA adducts and represent cytotoxicity. In addition, reactive oxidant species generated as a by-product of CYP-mediated metabolic processes may be also involved in the toxicity. Several CYP species involved in benzo[a]pyrene metabolism have been reported, but which CYP species mainly mediates benzo[a]pyrene cytotoxicity is still controversial [17,23,24]. CYP1A1/2, 1B1, 3A4, 2C8 and 2C9/10 are considered to be the candidates for benzo[a]pyrene metabolism. A cell strain derived from Hepa-1c1c7 cells lacking AhR expression proved to be benzo[a]pyrene-resistant [19], which suggests that the manifestation of benzo[a]pyrene cytotoxicity requires the AhR-mediated induction of particular CYPs, CYP1A1, CYP1A2, CYP1B1 and CYP3A4. In HepG2 cells, CYP1A1 was induced by omeprazole alone, but the high level of CYP1A1 induced by benzo[a]pyrene was not affected by the simultaneous omeprazole treatment (figs 2A,B and 3). These results suggest that activation of the AhR pathway by omeprazole could not be involved in the aggravation of benzo[a]pyrene cytotoxicity in HepG2 cells.

The EROD assay clearly showed that omeprazole inhibits the EROD activity (i.e. CYP1A1/1A2 activity) [25], in intact Hepa-1c1c7 cells (fig. 4C). The experiment using recombinant human CYPs revealed that omeprazole has potent inhibitory activity against CYP1A1 and CYP3A4, but not against CYP1A2 (fig. 6). The CYP1B1 activity was not measured, because this enzyme is not expressed in HepG2 cells [8,26]. These results suggest that omeprazole alleviated benzo[a]pyrene cytotoxicity by directly inhibiting the CYP1A1 and/or CYP3A4 enzymatic activity.

We examined the effects of ellipticine, a CYP1A1 inhibitor [27], and ketoconazole, a CYP3A4 inhibitor [28], on benzo[a]pyrene cytotoxicity to confirm which CYP dominantly contributes to the toxicity. Ketoconazole reduced benzo[a]pyrene cytotoxicity in Hepa-1c1c7 cells only at high doses (>10 μM) (fig. 5). However, it has been reported that ketoconazole inhibits CYP3A4 at much lower doses (<1 μM). For example, ketoconazole inhibits testosterone 11β-hydroxylation with IC_{50} value at 0.03 μM, and erythromycin *N*-demethylation with K_i value at 0.7 μM [29,30]. These results show that CYP3A4 should not contribute dominantly to benzo[a]pyrene cytotoxicity. In contrast, the CYP1A1 inhibitor ellipticine completely blocked benzo[a]pyrene cytotoxicity (fig. 5). The kinetic analysis revealed that omeprazole is a potent inhibitor of CYP1A1, because the affinity of omeprazole to the enzyme is stronger than that to

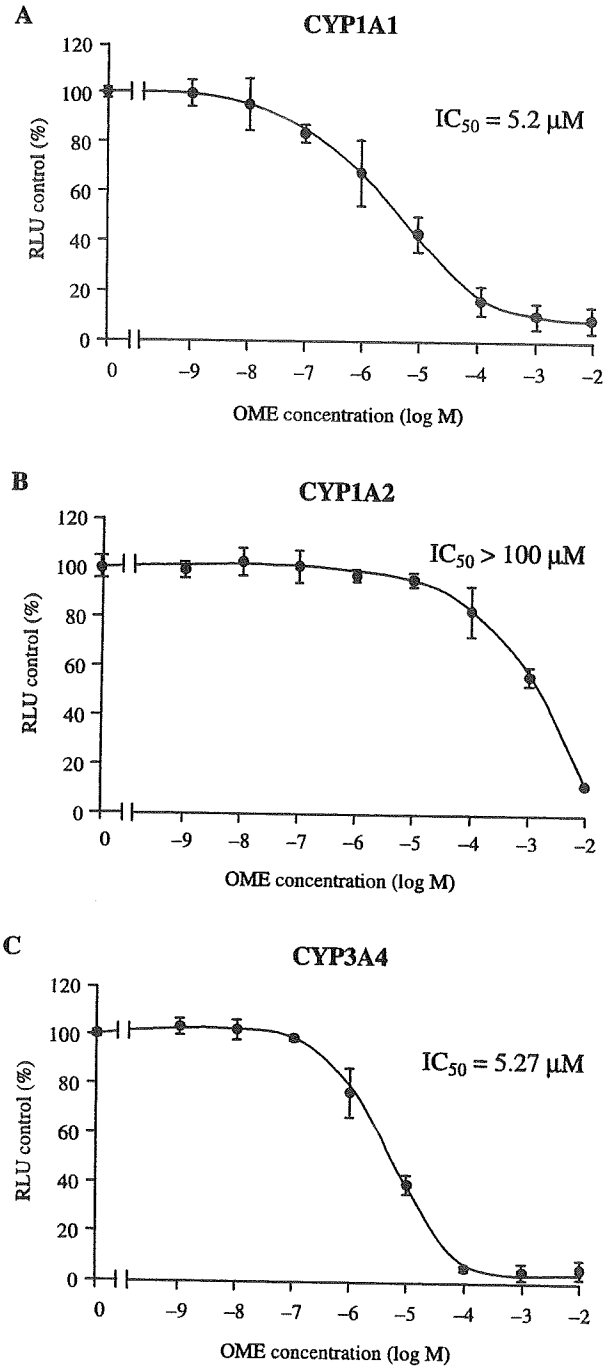

Fig. 6. Inhibition of recombinant human CYP activity by omeprazole (OME). CYP1A1 (A), 1A2 (B) and 3A4 (C) activity was determined using P450-Glo Assays and Sf9 cell microsomes containing recombinant human CYPs. Particular substrates and microsomes for each CYP were incubated at 37° for 30 min. with various concentrations of OME. The figure represents mean ± S.D. of triplicate determinations. RLU, relative light unit.

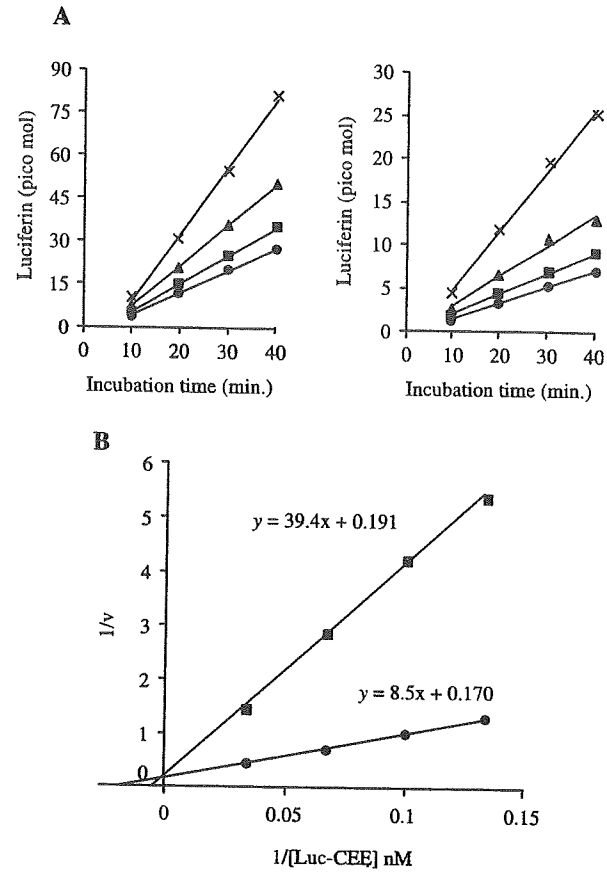

Fig. 7. Kinetic analysis of inhibition by omeprazole (OME) on human CYP1A1 activity. (A) CYP1A1 activity was determined using P450-Glo Assays and recombinant human CYP1A1 with various concentration of substrate in the absence (left) or presence (right) of OME. Assays were conducted in the presence of 10 μM OME and either 1 μM (●), 2.5 μM (■), 5 μM (▲) or 10 μM (×) of luciferin-6′-chloroethyl ether (Luc-CEE), and generated luciferin was measured every 10 min. for 40 min. Data shown are the mean of duplicate determinations from a single experiment. (B) Lineweaver–Burk plots of the CYP1A1 activity in the presence (●) or absence of 10 μM OME (■).

the substrate, that is, the K_i value (3.21 μM) is smaller than the K_m value (50.1 μM) (fig. 7). These results ensure that CYP1A1 dominantly contributes to benzo[a]pyrene cytotoxicity. We have determined the inhibition effect of omeprazole on CYP1A1 enzyme by using recombinant human CYP1A1. We expect mouse CYP1A1 also to be inhibited by omeprazole, because similar results of EROD activity inhibition were obtained in Hepa1c1c7 and HepG2 cells in our study (fig. 4).

Taken together, these findings indicate that omeprazole alleviates benzo[a]pyrene cytotoxicity by inhibiting the CYP1A1 activity in Hepa-1c1c7 and HepG2 cells. CYP1A1 is also a member of the CYP enzyme group that can be inhibited by omeprazole. The protection effect of omeprazole on the cytotoxicity of benzo[a]pyrene is more significant in Hepa1c1c7 than in HepG2 cells (fig. 1), although inhibition of EROD activity was comparable in both cell lines (fig. 4). Other causes, such as susceptibility to the reactive oxygen species, expression pattern of CYP species and the presence of omeprazole metabolites, may be involved in the protection effect, and these factors may be different between the two cell lines.

Figures 2 and 3 show that omeprazole concentration higher than 50 μM is required for the AhR-mediated CYP1A1 induction in HepG2 cells. This omeprazole concentration inhibits recombinant human CYP1A1 activity to less than 10% (fig. 6) and EROD activity in benzo[a]pyrene-treated HepG2 cells (fig. 4B). These results suggest that sufficiently high omeprazole concentrations to induce CYP1A1 inhibits CYP1A1 enzymatic activity, which in turn might indicate that omeprazole could not aggravate the effects of benzo[a]pyrene-type precarcinogens, which are chemicals metabolically activated by CYP1A1 through the AhR pathway.

Some phytochemicals, such as flavones and anthraquinone, have activities for both induction and inhibition of CYP1A1 [31–34]. Berberine, a plant isoquinoline alkaloid, has this 'biphasic effect' on CYP1A1 and has been used as a therapeutic agent like omeprazole [35]. To examine the aggravating effects of these chemicals on precarcinogens, it is necessary to carry out experiments similar to those of our present study.

Acknowledgements

This work was supported by the Environmental Technology Development Fund (Ministry of the Environment, Japan), Grant-in-aid for Scientific Research (Ministry of Education, Science, Sports and Culture, Japan) and Industrial Technology Research Grant Program in 2005 (New Energy and Industrial Technology Development Organization). We thank Mabel WL Chu for correcting English usage.

References

1 Lind T, Cederberg C, Ekenved G, Haglund U, Olbe L. Effect of omeprazole-a gastric proton pump inhibitor-on pentagastrin stimulated acid secretion in man. Gut 1983;**24**:270–6.
2 Ko J, Sukhova N, Thacker D, Chen P, Flockhart D. Evaluation of omeprazole and lansoprazole as inhibitors of cytochrome P450 isoforms. Drug Metab Dispos 1997;**25**:853–862.
3 Diaz D, Fabre I, Daujat M, Saint AB, Bories P, Michel H *et al.* Omeprazole is an aryl hydrocarbon-like inducer of human hepatic cytochrome P450. Gastroenterology 1990;**99**:737–47.
4 Curi-Pedrosa R, Daujat M, Pichard L, Ourlin JC, Clair P, Gervot L *et al.* Omeprazole and lansoprazole are mixed inducers of CYP1A and CYP3A in human hepatocytes in primary culture. J Pharmacol Exp Ther 1994;**269**:384–92.
5 Burbach KM, Poland A, Bradfield CA. Cloning of the Ah-receptor cDNA reveals a distinctive ligand-activated transcription factor. Proc Natl Acad Sci USA 1992;**89**:8185–9.
6 Denison MS, Fisher JM, Whitlock JP. Protein-DNA interactions at recognition sites for the dioxin-Ah receptor complex. J Biol Chem 1989;**264**:16478–82.
7 Reyes H, Reisz-Porszasz S, Hankinson O. Identification of the Ah receptor nuclear translocator protein (Arnt) as a component of the DNA binding form of the Ah receptor. Science 1992;**256**:1193–5.
8 Sutter TR, Tang YM, Hayes CL, Wo YY, Jabs EW, Li X *et al.* Complete cDNA sequence of a human dioxin-inducible mRNA identifies a new gene subfamily of cytochrome P450 that maps to chromosome 2. J Biol Chem 1994;**269**:13092–9.
9 Gu YZ, Hogenesch JB, Bradfield CA. The PAS superfamily: sensors of environmental and developmental signals. Annu Rev Pharmacol Toxicol 2000;**40**:519–61.
10 Daujat M, Peryt B, Lesca P, Fourtanier G, Domergue J, Maurel P. Omeprazole, an inducer of human CYP1A1 and 1A2, is not a ligand for the Ah receptor. Biochem Biophys Res Commun 1992;**188**:820–5.
11 Quattrochi LC, Tukey RH. Nuclear uptake of the Ah (dioxin) receptor in response to omeprazole: transcriptional activation of the human CYP1A1 gene. Mol Pharmacol 1993;**43**:504–8.
12 Kikuchi H, Hossain A, Sagami I, Ikawa S, Watanabe M. Different inducibility of cytochrome P-4501A1 mRNA of human and mouse by omeprazole in culture cells. Arch Biochem Biophys 1995;**316**:649–52.
13 Backlund M, Johansson I, Mkrtchian S, Ingelman-Sundberg M. Signal transduction-mediated activation of the aryl hydrocarbon receptor in rat hepatoma H4IIE cells. J Biol Chem. 1997;**272**:31755–63.
14 Backlund M, Ingelman-Sundberg M. Regulation of aryl hydrocarbon receptor signal transduction by protein tyrosine kinases. Cell Signal 2005;**17**:39–48.
15 Lemaire G, Delescluse C, Pralavorio M, Ledirac N, Lesca P, Rahmani R. The role of protein tyrosine kinases in CYP1A1 induction by omeprazole and thiabendazole in rat hepatocytes. Life Sci 2004;**74**:2265–78.
16 Okey AB, Dube AW, Vella LM. Binding of benzo(a)pyrene and dibenz(a,h)anthracene to the Ah receptor in mouse and rat hepatic cytosols. Cancer Res 1984;**44**:1426–32.
17 Gelboin HV. Benzo[a]pyrene metabolism, activation, and carcinogenesis: role and regulation of mixed-function oxidases and related enzymes. Physiol Rev 1980;**60**:1107–66.
18 Ko CB, Kim SJ, Park C, Kim BR, Shin CH, Choi S *et al.* Benzo(a)pyrene-induced apoptotic death of mouse hepatoma Hepa1c1c7 cells via activation of intrinsic caspase cascade and mitochondrial dysfunction. Toxicology 2004;**99**:35–46.
19 Zhang J, Watson AJ, Probst MR, Minehart E, Hankinson O. Basis for the loss of aryl hydrocarbon receptor gene expression in clones of a mouse hepatoma cell line. Mol Pharmacol 1996;**50**:1454–62.
20 Ekman L, Hansson E, Havu N, Carlsson E, Lundberg C. Toxicological studies on omeprazole. Scand J Gastroenterol Suppl 1985;**108**:53–69.
21 Salgueiro E, Rubio T, Hidalgo A, Manso G. Safety profile of proton pump inhibitors according to the spontaneous reports of suspected adverse reactions. Int J Clin Pharmacol Ther 2006;**44**:548–56.
22 Kennedy SW, Jones SP. Simultaneous measurement of cytochrome P4501A catalytic activity and total protein concentration with a fluorescence plate reader. Anal Biochem 1994;**222**:217–23.
23 Yun CH, Shimada T, Guengerich FP. Roles of human liver cytochrome P4502C and 3A enzymes in the 3-hydroxylation of benzo(a)pyrene. Cancer Res 1992;**52**:1868–74.
24 Nebert DW, Dalton TP, Okey AB, Gonzalez FJ. Role of aryl hydrocarbon receptor-mediated induction of the CYP1 enzymes in environmental toxicity and cancer. J Biol Chem 2004;**279**:23847–50.
25 Eugster HP, Probst M, Wurgler FE, Sengstag C. Caffeine, estradiol, and progesterone interact with human CYP1A1 and CYP1A2. Evidence from cDNA-directed expression in *Saccharomyces cerevisiae*. Drug Metab Dispos 1993;**21**:43–9.
26 Spink DC, Hayes CL, Young NR, Christou M, Sutter TR, Jefcoate CR *et al.* The effects of 2,3,7,8-tetrachlorodibenzo-p-dioxin on estrogen metabolism in MCF-7 breast cancer cells: evidence for induction of a novel 17 beta-estradiol 4-hydroxylase. J Steroid Biochem Mol Biol 1994;**51**:251–8.
27 Lesca P, Rafidinarivo E, Lecointe P, Mansuy D. A class of strong inhibitors of microsomal monooxygenases: the ellipticines. Chem Biol Interact 1979;**24**:189–97.
28 Sai Y, Dai R, Yang TJ, Krausz KW, Gonzalez FJ, Gelboin HV *et al.* Assessment of specificity of eight chemical inhibitors using

cDNA-expressed cytochromes P450. Xenobiotica 2000;**30**:327–43.

29 Choi MH, Skipper PL, Wishnok JS, Tannenbaum SR. Characterization of testosterone 11 beta-hydroxylation catalyzed by human liver microsomal cytochromes P450. Drug Metab Dispos 2005;**33**:714–8.

30 Rodrigues AD, Roberts EM, Mulford DJ, Yao Y, Ouellet D. Oxidative metabolism of clarithromycin in the presence of human liver microsomes. Major role for the cytochrome P4503A (CYP3A) subfamily. Drug Metab Dispos 1997;**25**:623–30

31 Sun M, Sakakibara H, Ashida H, Danno G, Kanazawa K. Cytochrome P4501A1-inhibitory action of antimutagenic anthraquinones in medicinal plants and the structure-activity relationship. Biosci Biotechnol Biochem 2000;**64**:1373–8.

32 Wang HW, Chen TL, Yang PC, Ueng TH. Induction of cytochromes P450 1A1 and 1B1 by emodin in human lung adenocarcinoma cell line CL5. Drug Metab Dispos 2001;**29**:1229–35.

33 Zhang S, Qin C, Safe SH. Flavonoids as aryl hydrocarbon receptor agonists/antagonists: effects of structure and cell context. Environ Health Perspect 2003;**111**:1877–82.

34 Chaudhary A, Willett KL. Inhibition of human cytochrome CYP 1 enzymes by flavonoids of St. John's wort. Toxicology 2006;**217**:194–205.

35 Vrzal R, Zdarilova A, Ulrichova J, Blaha L, Giesy JP, Dvorak Z. Activation of the aryl hydrocarbon receptor by berberine in HepG2 and H4IIE cells: Biphasic effect on CYP1A1. Biochem Pharmacol 2005;**70**:925–36.

BIOCHEMICAL PHARMACOLOGY 77 (2009) 660–669

available at www.sciencedirect.com

ScienceDirect

journal homepage: www.elsevier.com/locate/biochempharm

Review

Dioxin-induced toxicity on vascular remodeling of the placenta

Ryuta Ishimura [a,1], *Takashige Kawakami* [a,2], *Seiichiroh Ohsako* [b,a], *Chiharu Tohyama* [b,a,*]

[a] *National Institute for Environmental Studies, Tsukuba 305-8506, Japan*
[b] *Laboratory of Environmental Health Sciences, Center for Disease Biology and Integrative Medicine, Graduate School of Medicine, The University of Tokyo, Tokyo 113-00033, Japan*

ARTICLE INFO

Article history:
Received 31 July 2008
Accepted 15 October 2008

Keywords:
Angiogenesis
Arylhydrocarbon receptor
Hypoxia
Placenta
Vasculogenesis

ABSTRACT

Arylhydrocarbon receptor (AhR) activated by 2,3,7,8-tetrachlorodibenzo-*p*-dioxin (TCDD) triggers its downstream signaling pathway to exert adverse effects on vasculature development, which can be initiated by vasculogenesis, followed by angiogenesis, or vascular remodeling, in a variety of animals including avians, piscines and mammals. The placenta, a mammalian organ rich in vasculature, consists of endothelial and trophoblast cells of fetal origin, which proliferate and differentiate under hypoxic condition in the uterine horn. Our studies demonstrated that vascular remodeling occurs prominently in the placenta of the control Holtzman rat strain during the late period of gestation, and induces changes in cell shape and elimination by apoptosis of trophoblasts. As a result, the net volumes of both maternal and fetal blood in the placenta increase to cope with the essential requirements of oxygen and nutrients in the late period of gestation. On the other hand, *in utero* exposure to TCDD markedly suppressed the development of sinusoids and trophoblast cells and the apoptosis of trophoblast cells with a concomitant increase in the incidence of fetal death under hypoxic condition. A crosstalk between the hypoxia-inducible factor (HIF)-mediated pathway and AhR-mediated pathway is considered to play an important role in this physiological process. No such changes were observed in the Sprague–Dawley rat strain that turned out to have an AhR conformation identical to that of the Holtzman rat strain. In this commentary, we will discuss a possible link of the TCDD toxicities with the AhR signaling pathway and gestation-related diseases.

* *Corresponding author at:* Laboratory of Environmental Health Sciences, Center for Disease Biology and Integrative Medicine, Graduate School of Medicine, The University of Tokyo, 7-3-1 Hongo, Bunkyo-ku, Tokyo 113-0033, Japan. Tel.: +81 3 5841 1431; fax: +81 3 5841 1434.
E-mail address: mtohyama@mail.ecc.u-tokyo.ac.jp (C. Tohyama).
[1] Current address: The Jackson Laboratory, 600 Main Street, Bar Harbor 04609, USA.
[2] Current address: Tokushima-Bunri University, School of Pharmaceutical Sciences, Tokushima 770-8514, Japan.

Abbreviations: AhR, arylhydrocarbon receptor; ARNT, aryl hydrocarbon receptor nuclear translocator; GD, gestation day; HIF, hypoxia-inducible factor; HUVECs, human umbilical vein endothelial cells; TCDD, 2,3,7,8-tetrachlorodibenzo-*p*-dioxin.

0006-2952/$ – see front matter © 2008 Elsevier Inc. All rights reserved.
doi:10.1016/j.bcp.2008.10.030